T.R.
GEBZE TECHNICAL UNIVERSITY
GRADUATE SCHOOL OF NATURAL AND APPLIED SCIENCES

DESIGN OF DIGITALLY CONTROLLED LLC RESONANT CONVERTER

SERKAN DOĞANGÜNEŞ
A THESIS SUBMITTED FOR THE DEGREE OF
MASTER OF SCIENCE
DEPARTMENT OF ELECTRONICS ENGINEERING

GEBZE
2016

T.R.

GEBZE TECHNICAL UNIVERSITY

GRADUATE SCHOOL OF NATURAL ANDAPPLIED SCIENCES

DESIGN OF DIGITALLY CONTROLLED LLC RESONANT CONVERTER

SERKAN DOĞANGÜNEŞ

A THESIS SUBMITTED FOR THE DEGREE OF MASTER OF SCIENCE

DEPARTMENT OF ELECTRONICS ENGINEERING

THESIS SUPERVISOR

ASSOC. PROF. DR. ABDULKADİR BALIKÇI

GEBZE

2016

T.C.
GEBZE TEKNİK ÜNİVERSİTESİ
FEN BİLİMLERİ ENSTİTÜSÜ

SAYISAL KONTROLLÜ LLC REZONANS DÖNÜŞTÜRÜCÜ TASARIMI

SERKAN DOĞANGÜNEŞ
YÜKSEK LİSANS TEZİ
ELEKTRONİK MÜHENDİSLİĞİ ANABİLİM DALI

DANIŞMANI
DOÇ. DR. ABDULKADİR BALIKÇI

GEBZE
2016

GEBZE TEKNİK ÜNİVERSİTESİ	**YÜKSEK LİSANS JÜRİ ONAY FORMU**

GTÜ Fen Bilimleri Enstitüsü Yönetim Kurulu'nun ..19../..01...../2016. tarih ve ..2016../..05..... sayılı kararıyla oluşturulan jüri tarafından 04/02/2016 tarihinde tez savunma sınavı yapılan SERKAN DOĞANGÜNEŞ'in tez çalışması Elektronik Mühendisliği Anabilim Dalında YÜKSEK LİSANS tezi olarak kabul edilmiştir.

JÜRİ

ÜYE
(TEZ DANIŞMANI) : Doç. Dr. Abdulkadir BALIKÇI

ÜYE : Prof. Dr. M. Hakan HOCAOĞLU

ÜYE : Yrd.Doç.Dr. Uğur HASIRCI

ONAY

Gebze Teknik Üniversitesi Fen Bilimleri Enstitüsü Yönetim Kurulu'nun

...../...../..... tarih ve ...../..... sayılı kararı.

İMZA/MÜHÜR

SUMMARY

In this thesis, design and application of a digitally controlled LLC half-bridge resonant converter is realized. Basic principles of resonant converters, the advantages and disadvantages have been examined. Electronic circuit devices that form the LLC resonant converter, their behaviors and circuit's current and voltage waveforms in the fundamental operation modes were analyzed. The selection of the reactive components (L-L-C) that form basis of the resonant tank was explained through a design procedure. The reactive components calculation was made for a specific LLC resonant converter whose attributes are 120W output power, 420VDC input and 24VDC output voltage. Transient and AC simulations of the design were performed in LTSpice IV environment and the simulation results were examined in the light of design knowledge. In order to control the designed hardware with a digital controller, PID controller structure and tuning methods are described. The control parameters for tuning the controller were determined using MATLAB® Simulink and the simulation results were analyzed. The PID controller built in MATLAB® Simulink has been developed in STM32F429 microcontroller and the flow diagrams belong to control algorithm of the converter were displayed. Prototype hardware for the design that was verified with calculations and simulations was carried out and its test results related current and voltage waveforms were analyzed on a real experimental setup.

Key Words: Half Bridge LLC Resonant Converter, Digital Control, Soft Switching.

ÖZET

Bu çalışmada LLC yarım köprü rezonans dönüştürücünün sayısal kontrolcü ile tasarımı ve uygulaması gerçekleştirilmiştir. Rezonans dönüştürücülerin temel çalışma prensipleri, avantajları ve dezavantajları incelenmiş, LLC rezonans dönüştürücüyü oluşturan elektronik elemanlar ve bu elemanların çeşitli çalışma modlarındaki davranışları ile devreye ait gerilim ve akımlar analiz edilmiştir. LLC rezonans dönüştürücünün temelini oluşturan rezonans tank komponentlerinin (L-L-C) bir tasarım prosedürü üzerinden seçimi açıklanmıştır. 420V giriş ve 24V çıkışa sahip 120W gücünde bir LLC rezonans dönüştürücü için rezonans tank komponentlerinin hesabı yapılmıştır. Bu tasarımın LTSpice IV ortamında simülasyonu yapılmış ve simülasyon sonuçları, tasarım bilgileri ışığında incelenmiştir. Tasarımı yapılan donanımın sayısal kontrolcü ile kontrolü için PID kontrolör yapısı ve ayar yöntemleri açıklanmıştır. Bu ayar yöntemleri ile MATLAB® Simulink® kullanılarak kontrolcü parametreleri belirlenmiş ve simülasyon sonuçları incelenmiştir. MATLAB®'da tasarlanan kontrolcünün STM32F429 mikrodenetleyicisi üzerinde geliştirilmesi yapılmış ve kontrol algoritmasına ait akış diyagramları gösterilmiştir. Hesaplamalar ve simülasyonlar ile doğrulanan tasarımın prototipi hazırlanarak ilgili akım ve gerilim sonuçları gerçek deney düzeneği üzerinde analiz edilmiştir.

Anahtar Kelimeler: LLC Rezonans Dönüştürücü, Sayısal Kontrol, Yumuşak Anahtarlama.

ACKNOWLEDGEMENTS

This thesis owes its existence to the contribution, help and inspiration of many people. First of all, I would like to express my gratitude and appreciation to Assoc. Prof. Dr. Abdulkadir BALIKÇI for his guidance during my research. His support and suggestions have been valuable for the progress of this thesis content.

I would particularly like to acknowledge to Res. Asst. Murat CEYLAN for his time and valuable contributions on this thesis. He has been effectively interested in my study. I am very thankful for his patience.

I would also like to thank you to Pavo Tasarım and its general manager Kutsal ANIL for their supports.

Finally, special thanks are giving to my wife and my family for their unconditional support, love and continuous encouragement through the process of researching and writing this thesis. Thank you my wife.

TABLE of CONTENTS

LIST of ABBREVIATIONS and ACRONYMS

Abbreviations and Acronyms		Explanations
AC	:	Alternating Current
ADC	:	Analog to Digital Converter
BOM	:	Bill of Materials
DC	:	Direct Current
DMA	:	Direct Memory Access
DSP	:	Digital Signal Processing
EMI	:	Electromagnetic Interference
FHA	:	First Harmonic Approximation
FM	:	Frequency Modulation
MCU	:	Micro Controller Unit
MOSFET	:	Metal Oxide Silicon Field Effect Transistor
PFC	:	Power Factor Correction
PRC	:	Parallel Resonant Converter
PWM	:	Pulse Width Modulation
RISC	:	Reduced Instruction Set Computing
SMPS	:	Switch Mode Power Supply
SPRC	:	Series-Parallel Resonant Converter
SRAM	:	Static Random Access Memory
SRC	:	Series Resonant Converter
ZCS	:	Zero Current Switching
ZVS	:	Zero Voltage Switching

LIST of FIGURES

LIST of TABLES

1. INTRODUCTION

LLC resonant converter usage has become popular thanks to its great benefits such as impressive efficiency, higher power density in contrast to other DC-DC converter topologies in order to meet industry requirements on the higher efficiency and higher power density. The LLC resonant converter can work with wide input voltage range in order to provide hold up time requirement especially in the space and aircraft applications. Growing demand for higher power density and low profile, the switching frequency of the SMPS applications has been forced to increase for lower passive components. Higher switching frequency means that higher switching loss and lower efficiency. Hence to decrease switching loss, LLC resonant converter serves ZVS switching technique which minimizes the switching loss, switch stresses, reduces BOM cost and provides better EMI performance [Fang et al., 2012].

This thesis proposes an isolated DC-DC converter which employs digitally controlled LLC resonant converter design, analysis and implementation.

In chapter 2, four traditional resonant topologies with half bridge structure are evaluated for DC-DC converter applications and analyzed their characteristics, advantages and drawbacks.

In chapter 3, a typical LLC resonant converter in the half-bridge configuration, its operation principles, its circuit modeling using simplification methods and input-output relationship in terms of voltage are presented.

In chapter 4, reactive components are designed for specific LLC resonant converter and design considerations are evaluated based on the requirements.

In chapter 5, the LLC resonant converter hardware model is simulated and the simulation results compared to design solution in chapter 4 are observed.

In chapter 6, digital control principles are presented and PID controller simulation is carried out in MATLAB® Simulink. The designed PID controller is implemented in microcontroller and the software flow diagrams are examined.

Finally, the report of the test results belong to experimental setup is presented in chapter 7.

2. OVERVIEW OF RESONANT DC-DC CONVERTER TOPOLOGIES

Resonant converters connect a DC system to AC system using resonant L-C network combinations. The switches in a resonant converter create a square wave AC waveform from the DC link. This LC resonant tank eliminates refuse harmonic components from the square wave.

In this chapter four traditional resonant topologies with half bridge structure will be evaluated for DC-DC converter applications and will be analyzed their characteristics, advantages and drawbacks.

2.1. Series Resonant Converter

A series resonant converter is composed of half bridge switches, L_r-C_r-R_i series resonant network and equivalent load resistor as shown in Figure 2.1. Each switch consists of a transistor semiconductor device and an antiparallel body diode which is utilized as freewheeling diode for inductive loads in the half bridge configurations. The resonant inductor L_r and the resonant capacitor C_r are in series and form a series L-C resonant tank. In this converter, the series resonant tank is in series with the load R_i [Vorpérian, 1984].

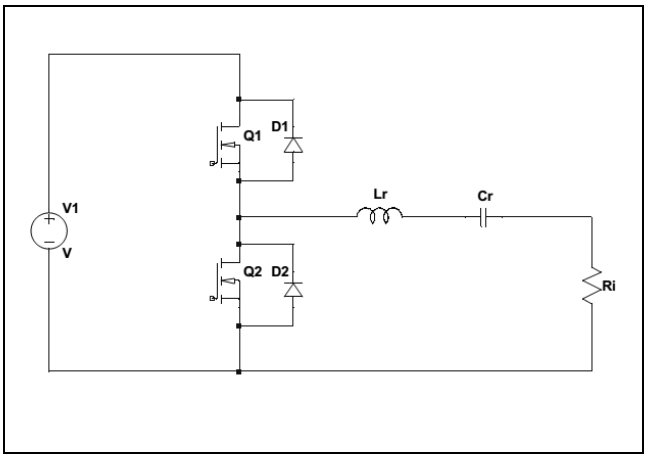

Figure 2.1: Series Resonant Converter.

As shown in Figure 2.1, L_r-C_r resonant tank and load R_i acts as a voltage divider. The resonant tank impedance changes in accordance with changing frequency of input voltage which is applied to resonant tank. In the fact that the impedance of the resonant tank and output load creates a voltage divider network and changing the high side impedance of the voltage divider determines the output voltage value. So when the resonant tank impedance is equal to zero, output voltage will be equal to input voltage. As a conclusion, a series resonant converter has a DC gain that is maximum 1 and can achieve this gain on the resonance frequency point.

The main advantage of the series resonant converters is simplicity of its structure and high efficiency at nominal input and full load. But series resonant converters cannot regulate the output voltage in the case of no load conditions because of the necessity for high switching frequency. They also have a drawback when the input voltage range is wide. In this case, nominal operating point will be far away from the resonance frequency and the efficiency of the converter reduces due to high circulating current.

2.2. Parallel Resonant Converter

A parallel resonant converter is composed of half bridge switches, L_r-C_r-R_i resonant network and equivalent load resistor as shown in Figure 2.2. Each switch consists of a transistor semiconductor device and an antiparallel body diode which is utilized as freewheeling diod for inductive loads in the half bridge configurations. In this topology resonant capacitor and resonant inductor are in series but resonant capacitor C_r is parallel with output load R_i [Vorpérian, 1984].

Advantage of the parallel resonant converter is that the converter can achieve operation in no load to full load conditions.

The main drawback of the parallel resonant converter is high circulating current at light load and low efficiency which arises due to this circulating current.

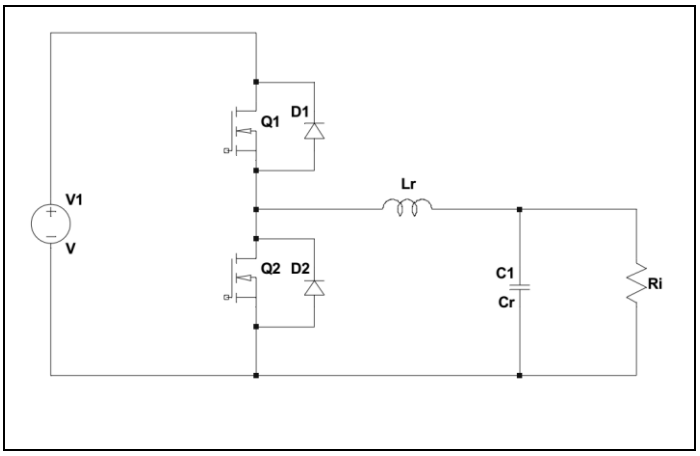

Figure 2.2: Parallel Resonant Converter.

2.3. Series-Parallel (LCC) Resonant Converter

A series-parallel resonant converter is a combination of a series resonant converter and a parallel resonant converter. The topology of this converter consists of a resonant tank which includes three resonant components L_r, C_s and C_p as shown in Figure 2.3.

The capacitor C_s is hooked up in series to resonant inductor L_r as in the series resonant converter. In addition to this connection, the capacitor C_p is hooked up in parallel to the AC load resistance R_i as in the parallel resonant converter.

Series-parallel resonant converter can achieve ZVS in the switching frequency which is higher than resonance frequency point.

Series-parallel resonant converter has narrow operation region in the meaning of switching frequency in comparison with the series resonant converter. This helps to lower conduction losses and better EMI performance [Vorpérian, 1984].

As mentioned before, the circulating current affects the converter efficiency directly. The circulating current in this topology is higher than series resonant converter and lower than parallel resonant converter.

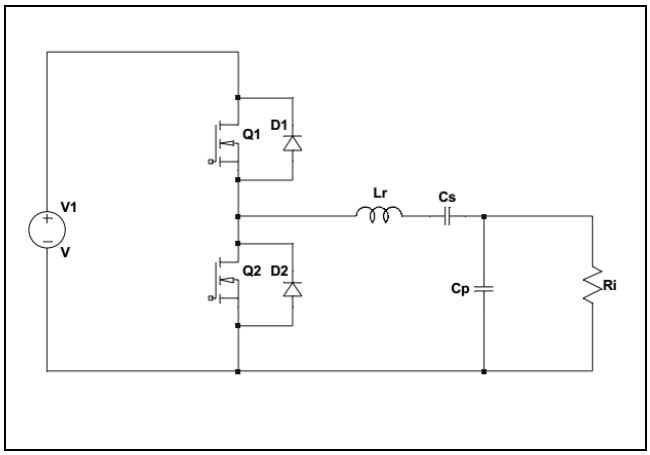

Figure 2.3: Series-Parallel Resonant Converter.

With above observation, series-parallel resonant converter incorporates good aspects of characteristics of SRC and PRC. But series-parallel resonant converter cannot eliminate wide input range operation drawback because of high conduction loss and switching loss.

2.4. LLC Resonant Converter

Three resonant converter topologies were examined in the previous sections and analyzed basic circuit structures, operation procedures, advantages and disadvantages. As a result, none of these three topologies are suitable for front-end operation in wide input voltage range because of high switching losses at light load conditions and high circulating current.

The limitations of the three converter topologies can be overcome by replacing with an inductor instead of parallel capacitor with the output load. The generated converter topology with these three reactive components is called LLC resonant converter in literature [Jung and Kwon, 2007]. The LLC resonant converter is composed of half bridge switches, resonant capacitor C_r, resonant inductor L_r, magnetizing inductor L_m and equivalent output load as shown in Figure 2.4.

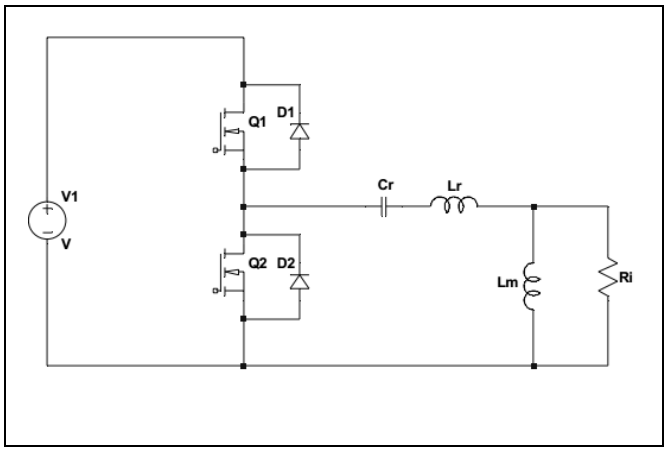

Figure 2.4: LLC Resonant Converter Topology.

LLC resonant converter topology has many advantages over the other resonant converter topologies. It can handle wide input range operation unlike the other topologies and regulate the output with frequency modulation in a short frequency range which depends on capacitor and inductors' values. Regardless of the output load, it can achieve zero voltage switching operation over the whole operation range. Therefore, it does not suffer from no load and light load conditions [Chen, 2011]. Usage of leakage and magnetizing inductance of a transformer can provide one integrated component for resonant and magnetizing inductance. It means that LLC resonant converter resonant tank can be composed of only two electrical components. In addition, an isolated DC-DC converter can be obtained with the usage of the transformer. This property is a great advantage for the systems, which are isolation is required between input and output.

For this reason, in this thesis LLC resonant converter design has been proposed with the integrated power transformer in conjunction with wide input voltage range and high efficiency objectives.

3. PRINCIPLES OF LLC RESONANT CONVERTER

This chapter presents a typical LLC resonant converter in the half-bridge configuration, its operation principles, its circuit modelling using simplification methods and input-output relationship in terms of voltage.

3.1. Construction of LLC Resonant Converter

The hardware circuit architecture of LLC half-bridge resonant DC-DC converter is depicted in Figure 3.1.

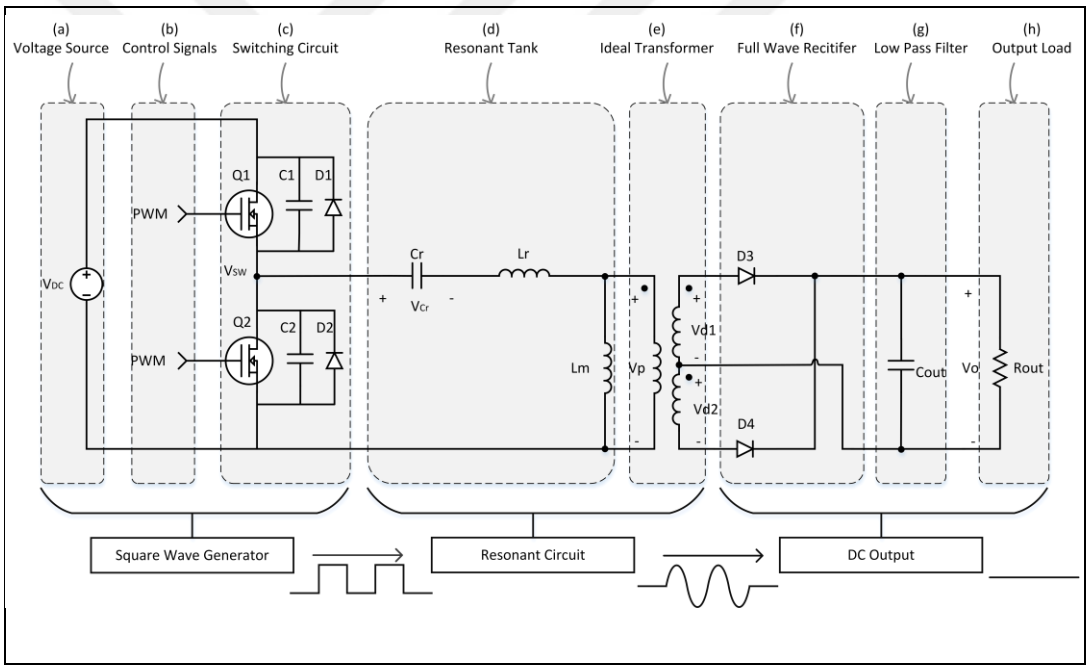

Figure 3.1: LLC Half-Bridge Resonant Converter Structure.

The circuit model is composed of DC voltage source, PWM control signals, half bridge switching circuit, LLC resonant tank, ideal transformer, full wave rectifier, output low pass filter and output load. The electrical and control model will be obtained from this simplified schematic and all parts of the structure are described below [MCI, 2010].

- Voltage Source

DC voltage source (V_{DC}) produces the nominal voltage to switching circuit. In general, this input voltage comes from the output of the PFC stage in the AC/DC converters or high voltage DC rail.

- Control Signals

Switching circuit is driven by complementary PWM signals that have 50% duty cycle and inserted very tiny dead time between sequential transitions that ensures zero voltage switching (ZVS) and shoot through prevention. PWM signals can be generated from an analog compensator or a digital controller regarding to control type.

- Switching Circuit

Half-bridge switching circuit is used in order to excite resonant tank generating square wave pulses. This switching circuit constitutes the backbone of the converter operation and affects directly efficiency, ruggedness and other performance requirements of the converter. Two MOSFETs (Q1, Q2) are used in the circuit as power switching device thanks to internal body diode (D1, D2), stray capacitances (C1, C2) necessary for ZVS operation, good high-frequency performance and high signal to noise ratio.

- Resonant Tank

The resonant tank circuit consists of L_r, C_r and L_m components that determine the electrical characteristics of LLC resonant topology. C_r is used for resonance capacitance and creates two-resonance frequency with resonant inductor and magnetizing inductor. The selection of these reactive components is the essential process of LLC resonance converter design and closely associated with overall system performance. Basically, resonant tank circulates the electrical current, so that the energy flows to output load through transformer [TI, 2010].

- Ideal Transformer

In the real life application, the integrated transformer includes resonance and magnetizing inductors. However, these inductors are depicted in block scheme

separately, the ideal transformer is demonstrated in order to show isolation and turns ratio between the input voltage and output voltage. Parasitic components of the transformer are neglected as shown in Figure 3.1.

- Full Wave Rectifier

Full wave rectifier converts the AC voltage in the transformer secondary side with the center-tapped configuration to DC voltage and is composed of two diodes.

- Low Pass Filter

The output capacitor performs as a low pass filter and creates the intended DC voltage with low ripple attribute.

- Output Load

R_{out} is the resistive component, which is a representation of output load. Therefore, output load is accepted as purely resistive load and all calculations is maintained with this assumption throughout this thesis.

3.2. FHA Analysis and Voltage Conversion Ratio

LLC resonant converter regulates the energy transfer from input source to output in accordance with the load.

"To design a converter for variable-energy transfer and output-voltage regulation, a voltage transfer function is a must." [TI, 2010]

This transfer function is the mathematical representation of the ratio of the output to input voltage and called as output voltage gain.

LLC resonant converter equations belong to the transfer function will be obtained using FHA (First Harmonic Approximation) technique and the transfer function of the converter will be derived relating converter model equations.

As mentioned before, switching circuit excites the LLC resonant tank with a square wave signal in the complementary mode. The converter gain relies on the frequency of the signal with 50% duty cycle. Therefore, the operating frequency is dependent on the output power rating. Due to the frequency is inversely proportional

to the power demand, the operating frequency increases with respect to low output power demand and vice versa. It means that lower power demand causes the operating point in the meaning of frequency goes away from the resonant point. On the other hand, the operating frequency approaches to resonant point in order to provide the higher power demand.

"The principle of the LLC operation assumes that the circuit operates close to its resonant frequency. Hence, sinusoidal variables are in play."[MCI, 2010]

For this reason, a great majority of the harmonics that belongs to resonating frequency is eliminated and LLC resonant tank acts as band pass filter for the input square wave.

In the view of such information, the current and voltage equations are derived from the converter model on the assumption that the considering only fundamental frequency by the aid of LLC resonant tank. This approach is called as the First Harmonious Approximation (FHA) and consists of considering its fundamental harmonic instead of the square wave signal. FHA technique ensures the analysis of the converter using traditional complex AC circuit analysis method and relies on the fundamental term of the Fourier Series reside in current and voltage of the input-output [MCI, 2010].

In the following computations, the Fourier Series is used in order to define the exciting square wave as a sinusoidal form. Due to this reason, it provides the analytical form of any periodic signal to be described in terms of an infinite sum of cosine or sine waveforms, whose frequencies are equal the fundamental frequency of the square wave and its integer multiples (harmonics).

Equation 3.1 shows the Fourier series of a square wave signal of amplitude A.

$$s(t) = \frac{A}{2} + 2 \cdot \frac{A}{\pi} \cdot \sum_{k=1,3,5,\dots} \frac{1}{k} sin\ (2\pi k f t) \qquad (3.1)$$

3.2.1. Switch Network Model

V_{sw} is the square wave output voltage of the switching circuitry that is depicted in the Figure 3.1, which is redefined from Fourier Series:

$$v_{sw}(t) = \frac{V_{dc}}{2} + 2 \cdot \frac{V_{dc}}{\pi} \cdot \sum_{k=1,3,5} \frac{1}{k} sin\ (2\pi k f_{sw} t) \tag{3.2}$$

where f_{sw} is the switching frequency and V_{dc} is the input DC voltage of the switching network.

The switching voltage is composed of the DC part that is $V_{dc}/2$ and infinite sum of sinusoidal waves. The DC part of the switching voltage is blocked by the resonant tank capacitor, C_r. The fundamental sine wave is obtained in case of k=1:

$$v_{sw,f}(t) = 2 \cdot \frac{V_{dc}}{\pi} \cdot sin\ (2\pi f_{sw} t) \tag{3.3}$$

The average, RMS and peak values of the fundamental frequency can be calculated from Equation 3.3 as shown in below:

$$\begin{aligned} v_{sw,\mathrm{f},av} &= 0, \\ v_{sw,\mathrm{f},RMS} &= \sqrt{2} \cdot \frac{V_{dc}}{\pi} \\ v_{sw,\mathrm{f},\mathrm{peak}} &= 2 \cdot \frac{V_{dc}}{\pi} \end{aligned} \tag{3.4}$$

where v_{sw} is voltage at the output of the switching circuit, *f* is consideration of the fundamental term only, peak is the peak square value, *av* is the average square value and *rms* is the root mean square value.

LLC resonant tank presents infinite impedance to the odd harmonics of the switching frequency except for the fundamental frequency, thanks to its nature; furthermore, the tank acts as finite impedance to the fundamental frequency. As a conclusion, a sinusoidal current waveform will appear in the resonant tank.

The reactive elements of the resonant tank create a phase shift between current and voltage as depicted in Figure 3.2. The tank circuit voltage leads the current by φ degree.

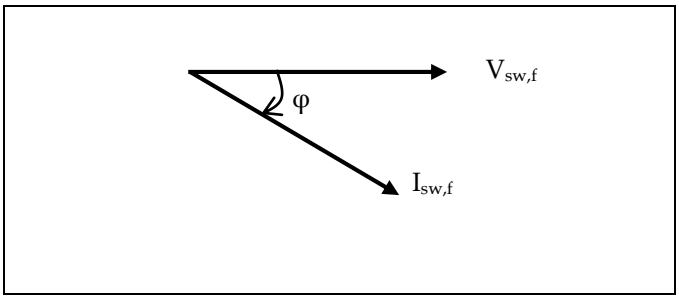

Figure 3.2: Voltage-Current Phase Delay.

Thus, the resonant tank current can be expressed as:

$$i_{r,f} = I_{r,f,peak} \sin\ (2\pi f_{sw} t - \varphi) \tag{3.5}$$

where *r* is the resonant tank, peak is the peak value, f is the fundamental value and φ is the phase shift between current and voltage.

When the high side MOSFET Q1 is turned on, V_{dc} that is input voltage supplies the current in Figure 3.3, which can be calculated as the average value as shown in below:

$$I_{dc} = \frac{1}{\pi} I_{r,f,peak}\ cos(\varphi) = \frac{\sqrt{2}}{\pi} I_{r,f,rms} cos(\varphi) \tag{3.6}$$

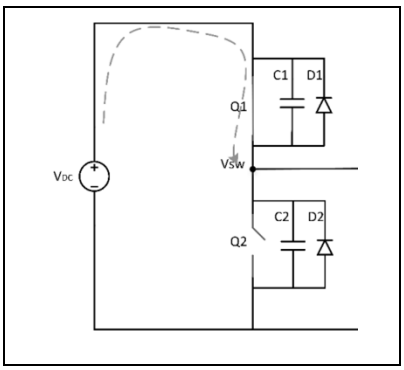

Figure 3.3: Switching Circuit When Q1 is ON.

An equivalent input switching circuit model can be derived using Equation 3.3, 3.5 and 3.6. This model will be used instead of real input switching network.

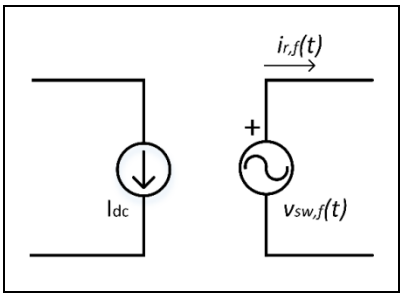

Figure 3.4: Switch Network Model.

The representation at the right performs the circuit that excites the resonant tank, where only sinusoidal signals at the fundamental frequency are of interest.

The circuit representation at the left right is composed of the imposed voltage and drawn current from V_{dc}.

Using this model, average input power equation takes form:

$$P_{dc,av} = \frac{\sqrt{2}}{\pi} V_{dc} I_{t,f,rms} \cos(\varphi) \tag{3.7}$$

3.2.2. Resonant Tank Model

In the real implementation, resonant tank is constructed by resonant capacitor and integrated transformer, which includes resonant inductor and magnetizing inductor. The resonant capacitor remains its position in the model. The real transformer is replaced by its model, where the magnetizing inductance (Lm) is clearly expressed. Leakage inductance in the secondary side will not be taken into the discussion, and is neglected throughout the modeling process [Huang et al., 2011].

As mentioned before, the focusing only fundamental sinusoidal frequency serves as basis for the modeling process. Thus, the transfer function of the resonant tank network (H(s)) can be derived from the model as shown in Figure 3.5. The equivalent resistor is used instead of the output load circuit.

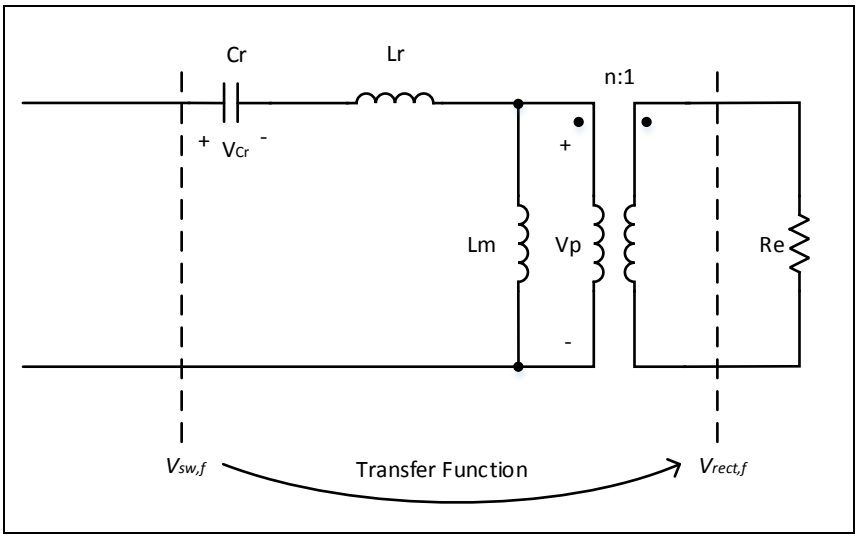

Figure 3.5: Resonant Tank Model Transfer Function.

The input impedance, $Z_{in}(s)$, is illustrated in Figure 3.6.

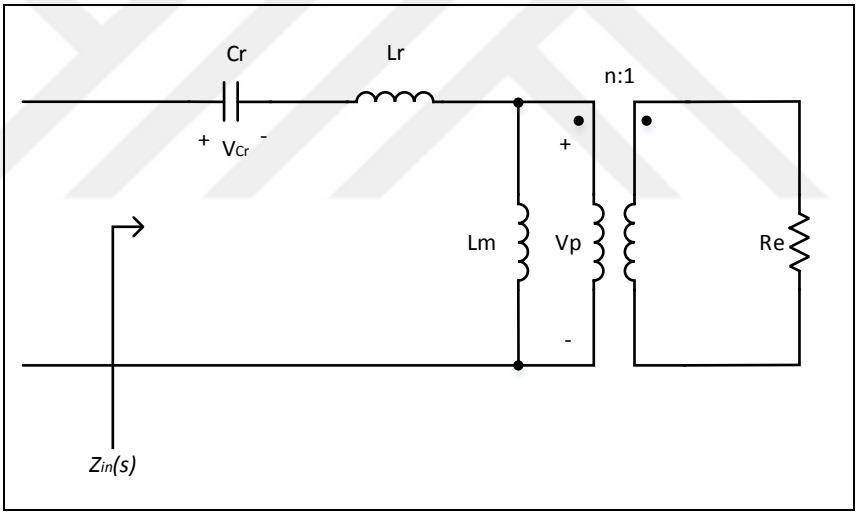

Figure 3.6: Resonant Tank Input Impedance.

The input impedance can be calculated with lumping the reactive components in the resonant tank into the series and parallel impedance as shown in Equation 3.8.

$$Z_{in}(s) = Z_s(s) + Z_p(s) \tag{3.8}$$

Z_s is the series impedance that includes C_r and L_r. Z_p is the parallel impedance that includes L_m, ideal transformer and equivalent resistor. $Z_s(s)$ and $Z_p(s)$ are expanded in the following equations, respectively.

$$Z_s(s) = \frac{1}{sC_r} + sL_r \tag{3.9}$$

$$Z_p(s) = (n^2 R_e)||sL_m \tag{3.10}$$

Using the equations above, the input impedance is computed:

$$\begin{aligned} Z_{in}(s) &= Z_s(s) + Z_p(s) \\ Z_{in}(s) &= \frac{1}{sC_r} + sL_r + (n^2 R_e)||sL_m \end{aligned} \tag{3.11}$$

where, n^2 is the ideal transformer turns ratio, as depicted in Figure 3.7.

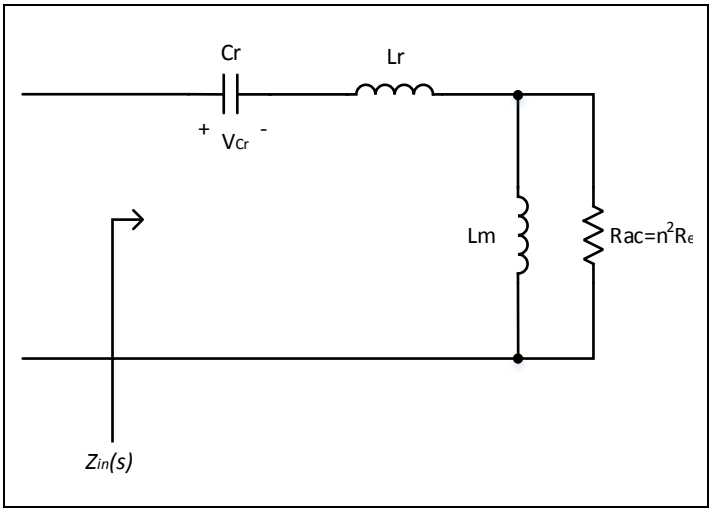

Figure 3.7: Resonant Tank Equivalent Model.

The circuit in Figure 3.5 can now be illustrated as a simplified two port model in Figure 3.8.

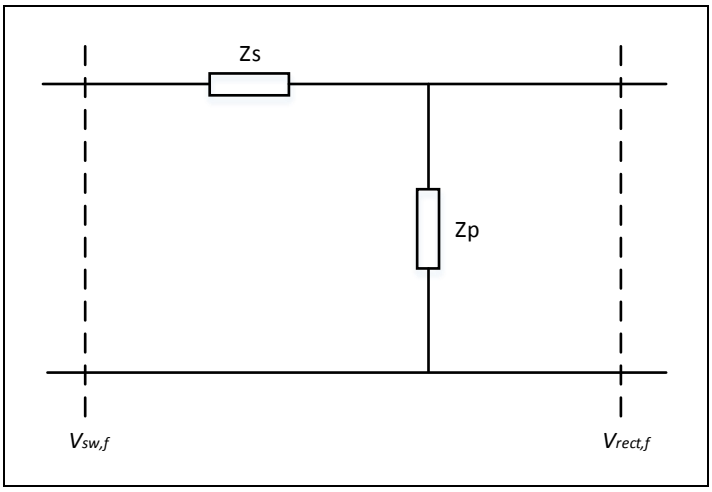

Figure 3.8: Simplified Resonant Tank Model.

In order to define the transfer function, the fundamental frequency is taken into consideration. Because the other frequencies are blocked by the resonant tank. Thus, the transfer function is derived:

$$H(s) = \frac{V_{rect,f,rms}}{V_{sw,f,rms}} = \frac{Z_p}{Z_p + Z_s} = \frac{(n^2 R_e)||sL_m}{nZ_{in}} \tag{3.12}$$

where $V_{rect,f,rms}$ is the rms value of the transformer secondary side, $V_{sw,f,rms}$ is the rms value of the resonant tank input stage.

The multiplier 1/n results from the secondary-primary voltage ratio that is expressed as follows:

$$v_{sec} = \frac{v_{prim}}{n} \tag{3.13}$$

3.2.3. Rectifier Model

The rectifier is composed of secondary side of the center-tapped transformer and two diodes. The rectifier operates full wave rectification process and converts the sinusoidal signal in the secondary side of the transformer to one of constant polarity pulsing signal. This sinusoidal signal is the conversion of the LLC resonant tank output through the transformer.

The current flows alternately through D3 and D4 diodes dependent on its sign as shown in Figure 3.9 and Figure 3.10 respectively.

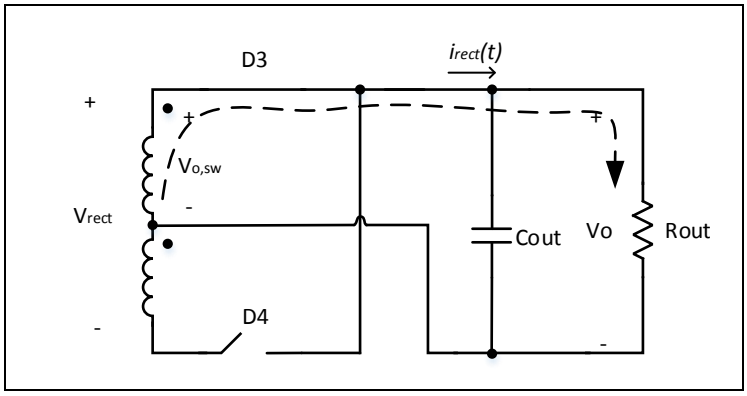

Figure 3.9: D3 Diode is Forward Biased When $i_{rect}(t)>0$.

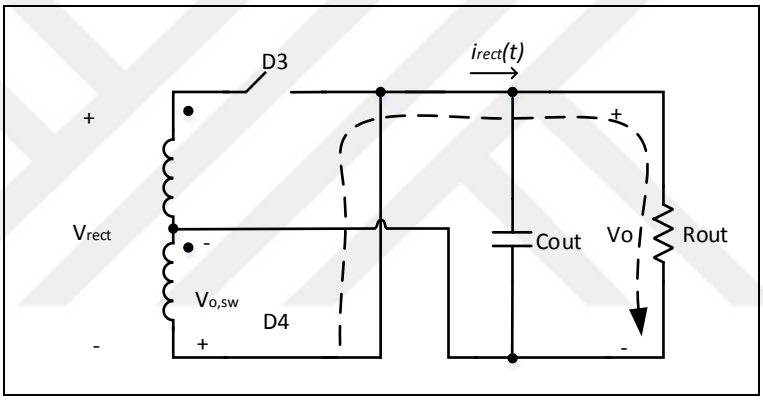

Figure 3.10: D4 Diode is Forward Biased When $i_{rect}(t)<0$.

If $i_{rect}(t)$ is positive, only D3 diode is forward biased and turns on. In addition, $v_{rect}(t)$ is equal to Vo. On the contrary, If ir(t) is negative, only D4 diode is forward biased and turns on. In additional, $v_{rect}(t)$ is equal to -Vo. $v_{rect}(t)$ is the output voltage value of the secondary side.

Considering the Fourier series of this square wave, centered around 0V, its analytical equation can be written (at the rectifier input), as in the following equation.

$$v_{rect}(t) = \frac{4}{\pi} V_o \sum_{k=1,3,5\ldots} \frac{1}{k} sin(2\pi k f_{sw} t - \partial) \qquad (3.14)$$

where ∂ is the phase lag relative to the input voltage.

The fundamental component is as follows

$$v_{rect,f}(t) = \frac{4}{\pi} V_o sin(2\pi k f_{sw} t - \partial) \quad (3.15)$$

The rms and average values of the fundamental component are given by

$$V_{rect,f,peak} = \frac{4}{\pi} V_o$$

$$V_{rect,f,avg} = 0 \quad (3.16)$$

$$V_{rect,f,peak} = \frac{2\sqrt{2}}{\pi} V_o$$

The current value after rectifier diodes is equal to absolute value of the fundamental component of the rectifier input current as shown in the following equation.

$$i_{rect,f,out}(t) = |i_{rect,f}(t)| \quad (3.17)$$

While the rectifier input current at the fundamental frequency is expressed in

$$i_{rect,f}(t) = I_{rect,f,peak} sin(2\pi f_{sw} t - \partial) \quad (3.18)$$

and output current of the rectifier is shown in

$$i_{rect,f,out} = I_{rect,f,peak} |sin(2\pi f_{sw} t - \partial)| \quad (3.19)$$

The average value of the rectifier output current is computed as

$$i_{rect,f,out,avg} = I_o = \frac{2}{\pi} I_{rect,f,pk} \quad (3.20)$$

where, I_o is the average flowing current into the output load.

Thanks to voltage and current of the rectifier are in phase, it is possible to replace the rectifier with a resistive element such as resistor. The equivalent resistor instead of the rectifier can be derived from Equation 3.16 to Equation 3.20 as shown in

$$R_e = \frac{v_{rect,f}(t)}{i_{rect,f}(t)} = \frac{2}{\pi I_o}\frac{4V_o}{\pi} = \frac{8}{\pi^2}R_o \tag{3.21}$$

The rectifier model is shown in the following figure.

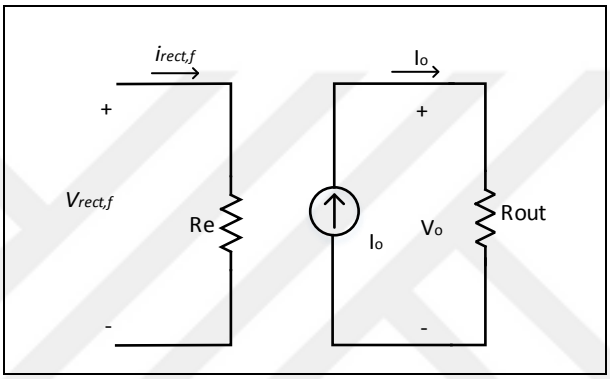

Figure 3.11: Full Wave Rectifier Model.

3.2.4. Converter Model

Up to this point, all stages belong to converter in Figure 3.1 are defined individually with the FHA approach and its model equations are derived using these definitions. Thus, overall converter model can be generated combining the model equations as shown in Figure 3.12.

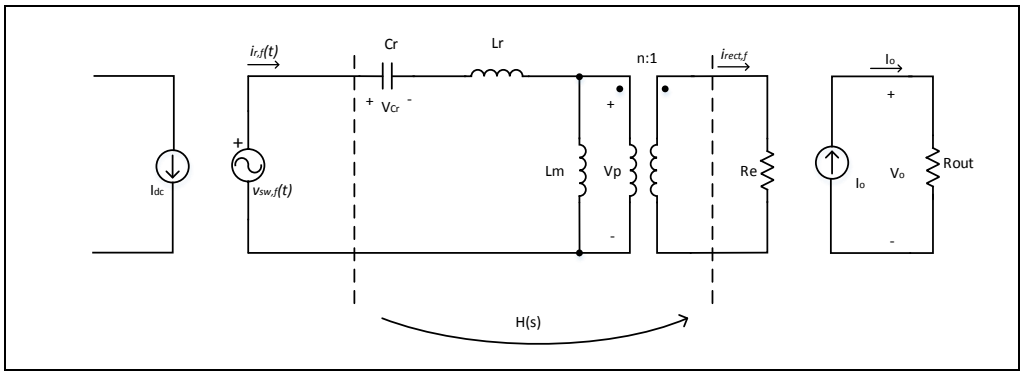

Figure 3.12: Overall Converter Model.

Equation 3.22 expresses the complete input-output relationship and it is defined as output to input ratio in terms of DC voltage.

$$\frac{V_o}{V_{dc}} = \frac{V_o}{V_{rect,f,rms}} \frac{V_{rect,f,rms}}{V_{sw,f,rms}} \frac{V_{rect,f,rms}}{V_{dc}}$$
$$= \frac{V_o}{\frac{2\sqrt{2}V_o}{\pi}} H(s) \frac{\frac{\sqrt{2}V_{dc}}{\pi}}{V_{dc}} = \frac{1}{2} H(s) \tag{3.22}$$

The voltage conversion ratio relies on Equation 3.23 and can be defined in Equation 3.24. It is clear that the voltage conversion ratio is similar to one-half of the forward transfer function.

$$M(f_{sw}) = n|H(s)| \tag{3.23}$$

$$\frac{V_o}{V_{dc}} = \frac{M(f_{sw})}{2n} \tag{3.24}$$

3.3. Voltage Conversion Ratio

LLC resonant tank has two resonant frequencies, which are generated by the C_r, L_r and L_m reactive components. One of them ($f_{r,1}$) occurs due to L_r and C_r. When the switching frequency goes down from $f_{r,1}$, Lm participates to resonance operation

and second one ($f_{r,2}$) occurs due to L_m, L_r and C_r. This is the result for LLC resonant converter belongs to multi resonant converters family [TI, 2010].

$f_{r,1}$ is the fundamental resonance frequency, so it will be called as resonance frequency (f_r) in definitions and is expressed as

$$f_r = \frac{1}{2\pi\sqrt{L_r C_r}} \tag{3.25}$$

$f_{r,2}$ secondary resonance frequency is shown in

$$f_{r,2} = \frac{1}{2\pi\sqrt{(L_r + L_m)C_r}} \tag{3.26}$$

The normalized frequency is used to simplify voltage gain equations and defined as the ratio of switching frequency to resonance frequency as

$$f_n = \frac{f_{sw}}{f_r} \tag{3.27}$$

The characteristic impedance, inductance rapport and the quality factor alter directly the voltage conversion ratio and they are expressed in the following equations, respectively.

$$Z_o = \sqrt{\frac{L_r}{C_r}} = \frac{1}{2\pi f_r C_r} = 2\pi f_r L_r \tag{3.28}$$

$$\lambda = \frac{L_r}{L_m} \tag{3.29}$$

$$Q = \frac{Z_o}{R_e} = \frac{\pi^2 Z_o I_{out}}{8n^2 V_{out}} \tag{3.30}$$

In order to calculate voltage conversion ratio, Equation 12 and Equation 23 are used and the result is shown in

$$M(f_{sw}) = m(f_n, \lambda, Q)$$

$$= \frac{1}{\sqrt{(1 + \lambda - \frac{\lambda}{{f_n}^2})^2 + Q^2(f_n - \frac{1}{f_n})^2}} \tag{3.31}$$

This means that the voltage transfer ratio is a complex function of the reactive component values and the normalized frequency. Thus, all parameters belong to conversion function for a specialized design must be computed before transfer ratio computation process. Although it seems to a strict restriction for considering voltage transfer ratio, it is possible to observe its curves using constant Q and λ values.

Figure 3.13 shows clearly the resonance frequency (f_r) in case of normalized frequency and gain values are equal to one. When the normalized frequency approaches to lower frequencies, the gain increases because of the second resonance frequency effect.

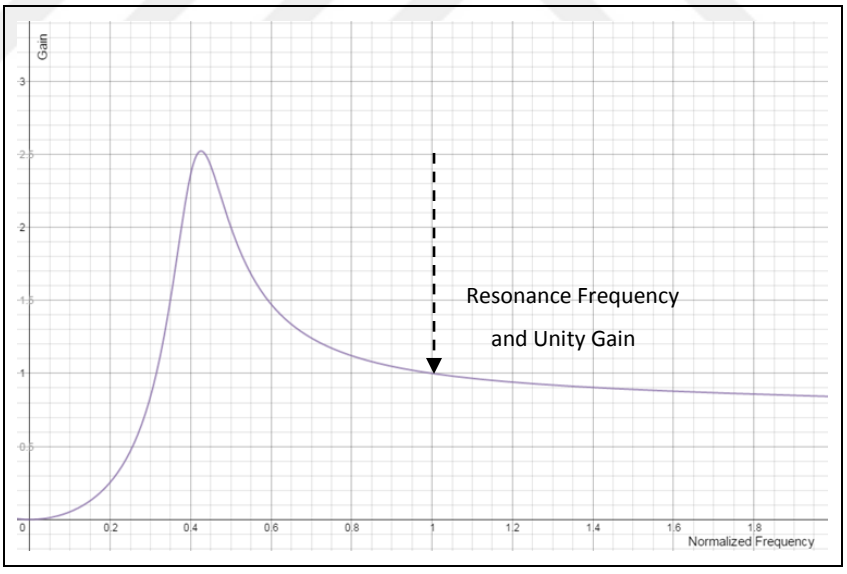

Figure 3.13: Voltage Conversion Ratio.

Figure 3.14 plots a group of curves obtained according to λ equals to 0.2 and Q varying from 0.2 (purple curve) to 1.8 (green curve) in 0.2 steps.

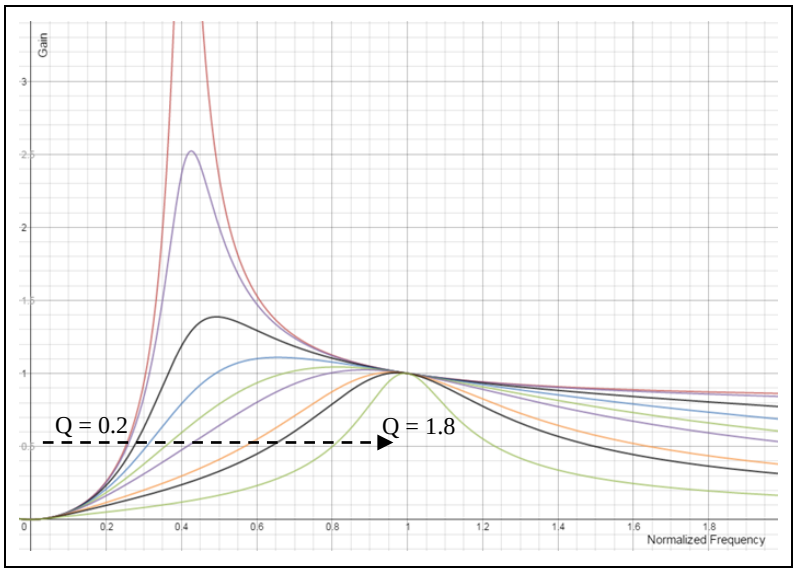

Figure 3.14: Voltage Conversion Ratio with Variable Q.

Figure 3.15 plots a group of curves obtained according to Q equals to 0.3 and λ varying from 0.1 (purple curve) to 0.9 (green curve) in 0.1 steps.

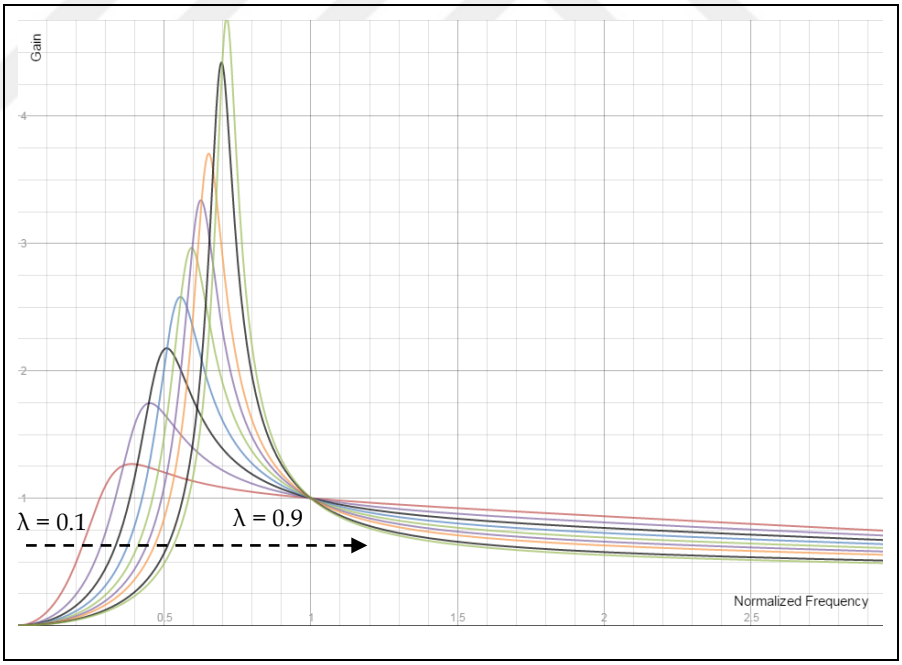

Figure 3.15: Voltage Conversion Ratio with Variable λ.

From the gain curves, some conclusions can be observed as follows:

- When Q decreases, the curve becomes gradually sharp.

- When λ increases, the curve becomes more and more flat.

In the design stage of the LLC resonant converter, these observations will be used according to some trade-offs. Additionally, the parameters are selected so that the converter operates at the resonance frequency for the nominal input voltage. Equation 3.24 can be derived for this operating point as shown in Equation 3.32.

$$M(f_r) = 2n\frac{V_{o,nom}}{V_{in,nom}} = 1 \tag{3.32}$$

The turns ratio is calculated from Equation 3.32 and given in the following equation.

$$n = \frac{V_{in,nom}}{2V_{o,nom}} \tag{3.33}$$

Analyzing the curves in Figure 3.14 and Figure 3.15, it is observed clearly that each curve crosses at the same point, which corresponds to resonance frequency f_{sw}=f_r. Furthermore, the conversion ratio is 1 at this point. Therefore, this point is called as load independent point and properly selected turns ratio provides the intended output voltage at nominal input voltage for any specific M curve.

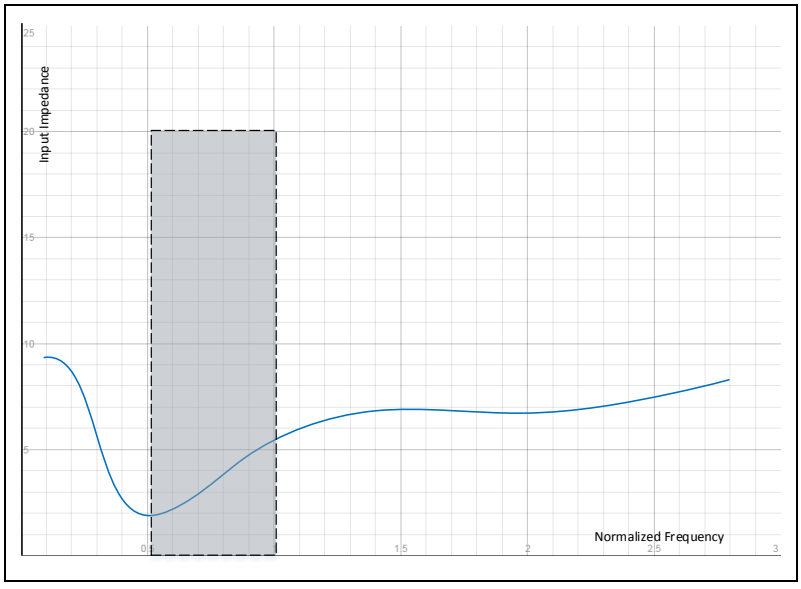

Figure 3.16: Normalized Input Impedance Magnitude.

Figure 3.16 shows the input impedance characteristic (defined Z_{in} in Figure 3.6) of the converter model. An area of the plane has been marked in the figure, where the curve has positive slope and the normalized switching frequency is lower than 1. Considering an inductor transfer function, it presents same characteristic and LLC circuit behaves as an inductor to input sinusoidal waveform and input circuit. Maintaining this operation in this area is mandatory in order to provide minimum switching losses [Liu, 2007]. In contrary, the part of the impedance curve that has negative slope presents capacitive characteristics. A point can be determined for each curve, which indicates the border between capacitive and inductive regions. Adding these points end to end, the red dotted line can be obtained as border line as shown in Figure 3.17. Additionally, the yellow marked area is determined by the border and assures that the converter maintains the operation in inductive region when the switching frequency is lower than resonance frequency.

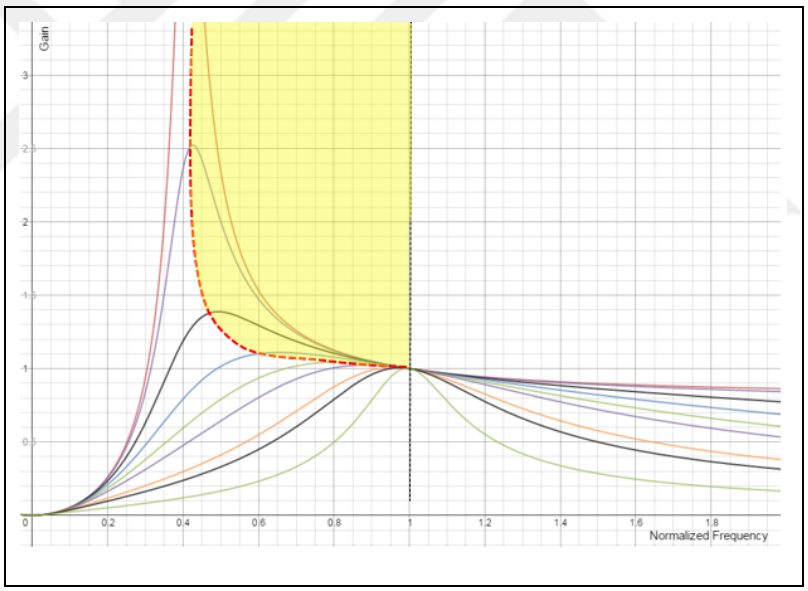

Figure 3.17 Border of Capacitive-Inductive Regions.

On the other hand, the marked area is limited by the Q parameter. Because Q is always higher than zero, which represents the no-load condition. This limitation is illustrated in Figure 3.18.

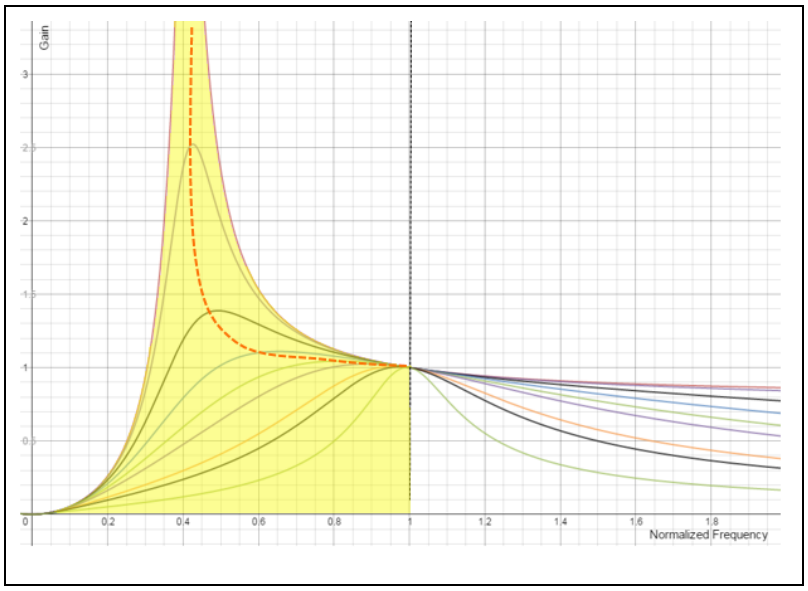

Figure 3.18 Operating Area Limited by Q=0.

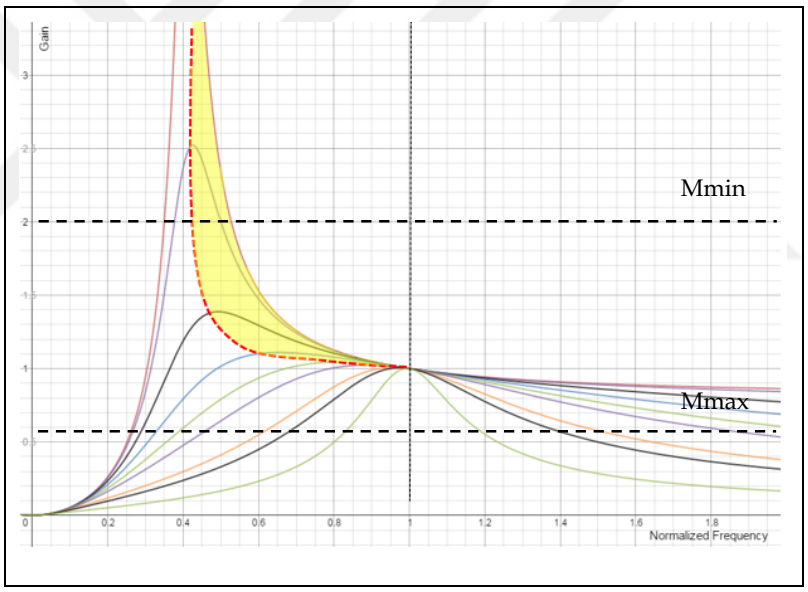

Figure 3.19 Gain Limitations And Intersection Area.

Similarly, the minimum and maximum gain requirements draw the border line at y-axis. They are expressed in Equation 3.34 and 3.35 according to min-max input voltage values and depicted in Figure 3.19 with the intersection area of Figure 3.17 and Figure 3.18.

$$M_{min}(f) = 2n\frac{V_o}{V_{in,max}} \tag{3.34}$$

$$M_{max}(f) = 2n\frac{V_o}{V_{in,min}} \tag{3.35}$$

As a conclusion, all acceptable operating areas can be associated in a single operation region as shown in Figure 3.20. Obviously, when the switching frequency is higher than the resonance frequency, the converter can provide ZVS operation and this area is valid for the normal operation.

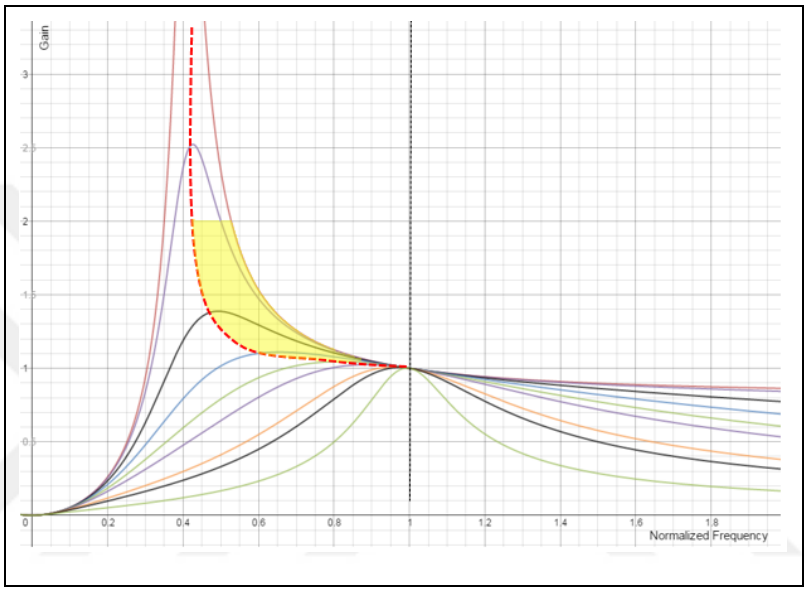

Figure 3.20 Final Operating Area.

3.4. Fundamental Operation Modes and Start-up of LLC Resonant Converter

In this chapter, LLC converter operation modes will be analyzed based on the resonance frequency [Kandrac et al., 2012]. Switching transitions and current flows are presented for each operation modes. Before focusing to operation modes, soft switching transition approach is considered for the MOSFETs turn on situation.

3.4.1. Zero Voltage Switching Approach

In order to reduce the volume of the reactive components such as capacitor and transformer for the LLC converter, it is intended to operate in high frequencies as

much as possible. But this causes high switching losses and reduces the overall converter efficiency. To eliminate this switching loss, ZVS is provided for the primary side MOSFETs [Chen et al., 2010].

ZVS is maintained only in the inductive region for the LLC resonant converter because of the tank voltage leads the tank current in the inductive region. The half bridge part of the circuit is considered for the ZVS and the related circuit is shown in Figure 3.21.

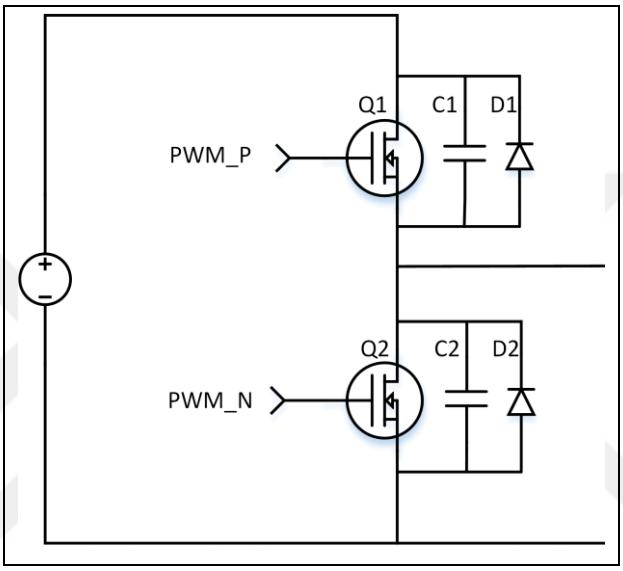

Figure 3.21: Half Bridge Circuit For ZVS Consideration.

C1 and C2 are the equivalent capacitors of the system which include drain-source capacitance, PCB stray capacitance, lead capacitance, etc. D1 and D2 are anti-parallel diodes of the MOSFETs.

Resonant tank current and gate to source voltage of the MOSFETs are depicted in Figure 3.22. Current flow directions and component positions are analyzed according to t0 through t4 time interval given below:

- t0 to t1 : Q1 and Q2 remains ON and OFF states, respectively. C2 capacitor is charged with Vdc.
- t1: Q1 is opened and D2 is forward biased. The current starts to flow through D2 as shown in Figure 23.
- t1 to t2 : Current remains the previously direction. Drain to source voltage of Q2 MOSFET is similar to D2 forward voltage and close to zero. Q2 can be turned

“ON” in this time interval and the switching loss will be close to zero because of the power calculation is the product of current and voltage.

- t2 : Q2 is closed and current flows reverse direction through Q2 instead of D2 in Figure 24.
- t2 to t3 : Current remains the previously direction and C1 capacitor is charged with V_{dc}.
- t3 : Q2 is opened and D1 is forward biased. The current flows through D2 as shown in Figure 25.
- t3 to t4 : Current remains the previously direction. Drain to source voltage of Q1 MOSFET is similar to D1 forward voltage and close to zero. Q1 can be turned “ON” in this time interval and the switching loss will be close to zero because of the power calculation is the product of current and voltage.
- t4 : Q1 is closed and current flows reverse direction through Q1 instead of D1 in Figure 26.

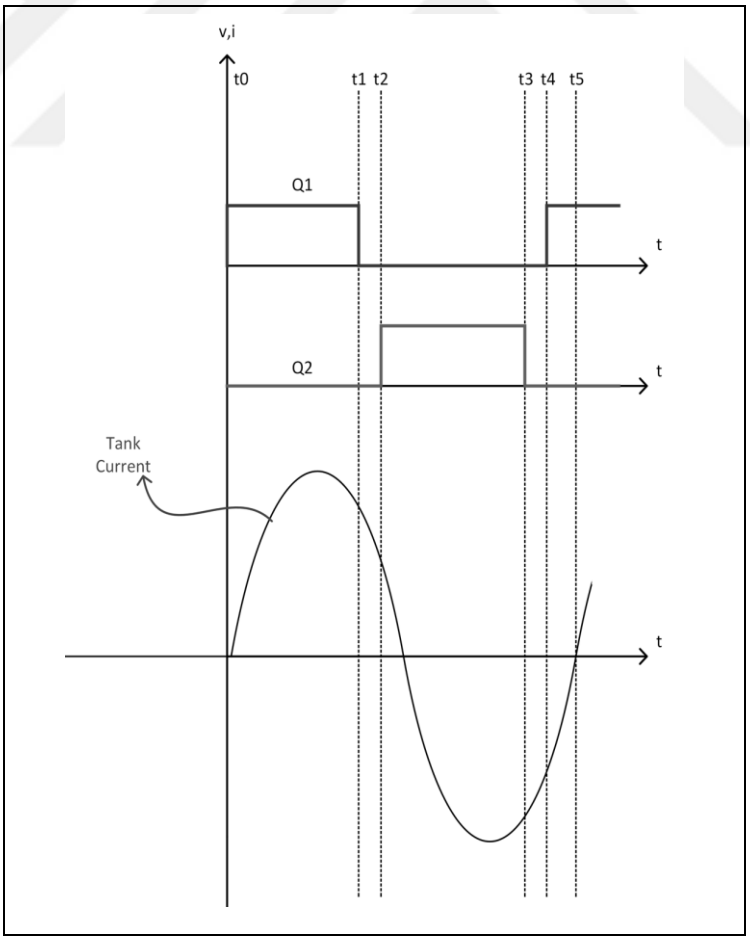

Figure 3.22: Tank Current and MOSFET’s VGS States.

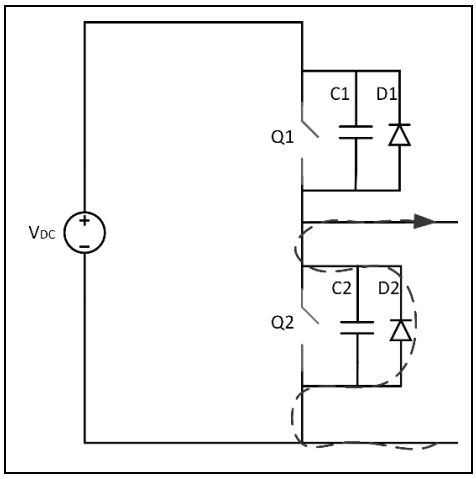

Figure 3.23: Current Direction for t1 to t2.

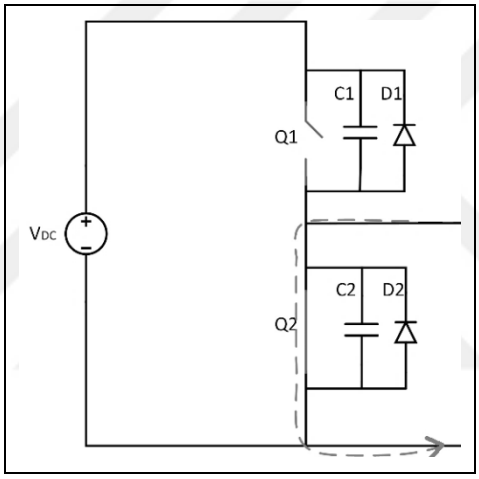

Figure 3.24: Current Direction for t2 and t2 to t3.

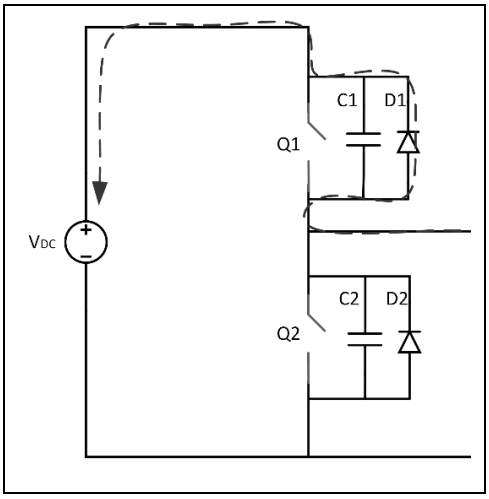

Figure 3.25: Current Direction for t3 and t3 to t4.

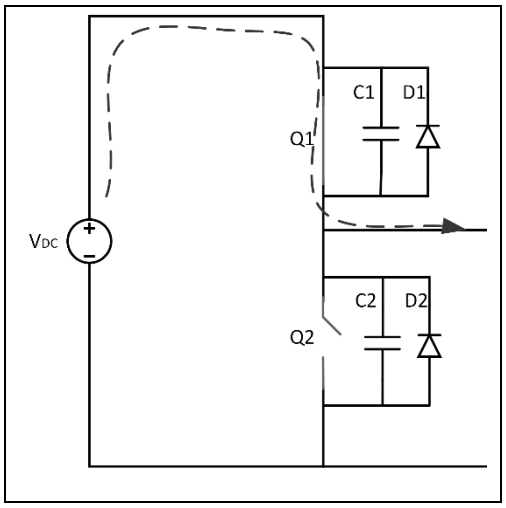

Figure 3.26: Current Direction for t4.

3.4.2. Operation at Resonance

This section presents the operation principles when the LLC resonant converter operates at the resonance frequency (f_r). Operation waveforms, current flow directions and component conditions are analyzed for six fundamental subintervals. All voltage and current waveforms are illustrated in Figure 3.27. Operation circuit belongs to each subinterval and its voltage and current directions are depicted from Figure 3.28 to Figure 3.33 [Yu et al., 2012].

- t0 to t1: Q1 is ON and Q2 is OFF state. The current flows from the input voltage source to the resonant tank. Resonant tank is charged and the load is supplied by input source throughout Q1. D3 diode is forward biased. L_m is shorted by the output resistance reflected to the primary side of the transformer, so Lm doesn't participate to resonance operation. The voltage value accoss the L_m (V_p) is nVout. D4 diode is reverse biased with -2Vout voltage value. Resonant tank current (I_r) starts to decay after it reaches to maximum value.
- t1 to t2: Q1 turns off at t1. Q1 is OFF and Q2 is OFF state. This subinterval is called as the dead time period and it prevents undesired the shoot through conduction between both MOSFETs. The node HB decays (C2 capacitor discharges) from V_{dc} to 0 and anti-parallel diode (D2) of the Q2 conducts. V_p reverses to -nVout. D3 and D4 diodes are reverse biased.

• t2 to t3: Q2 MOSFET is switched on at t2. I_r current flows Q2 instead of D2 and Q2 operates at third quadrant which means that the current flows source to drain. D4 starts to conduct and D3 is reverse biased. When IR =0, this phase ends.

• t3 to t4: Q1 is OFF, Q2 is ON state. I_r becomes negative after t=t3. D4 remains ON state and the voltage across D3 is equal to -nVout. At t4, IR reaches its minimum value.

• t4 to t5: Q2 turns off at t4 and this subinterval is reverse of the cycle in t1 to t2. C1 capacitor discharges and D1 diodes starts to conduct.

• t5 to t6: Q1 is switched on at t = t5. The I_r current starts to flow Q1 instead of D1. Similar to phase t2 to t3, current flows from source to drain of Q1 and the operating point of Q1 is third quadrant. The resonant tank supplies the input source and D3 diode is conducting.

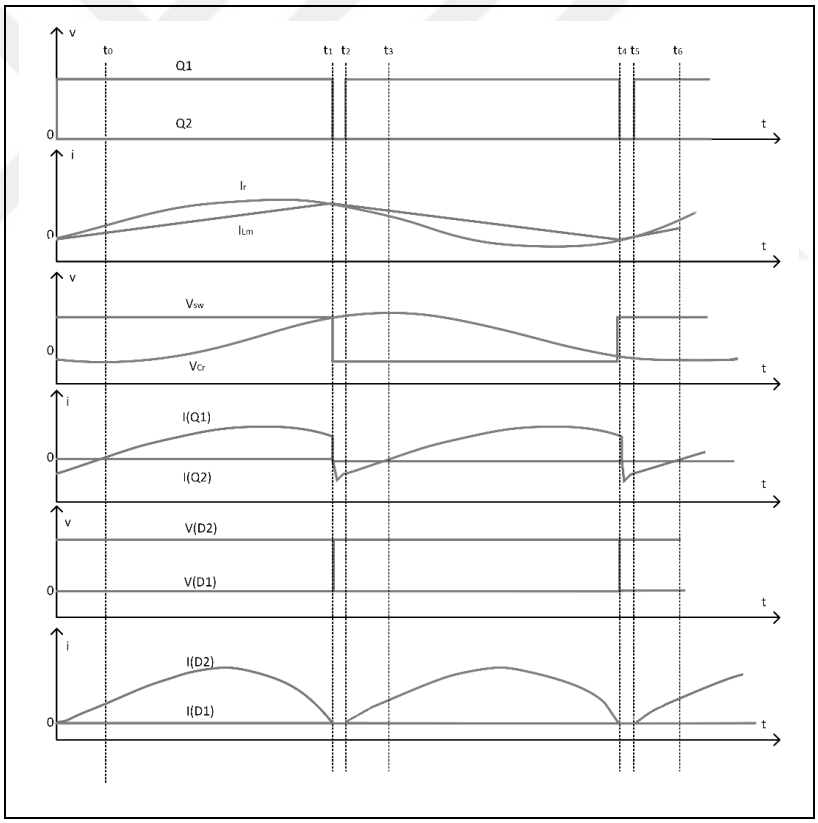

Figure 3.27: Voltage and Current Waveforms at $f_{sw}=f_r$.

Next switching cycle start at t=t6, so that this phase ends when IR=0.

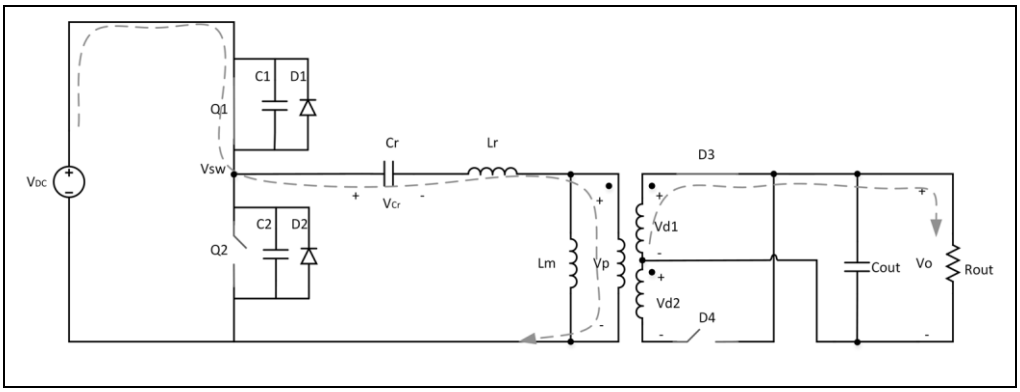

Figure 3.28: Circuit Operation for t0 to t1.

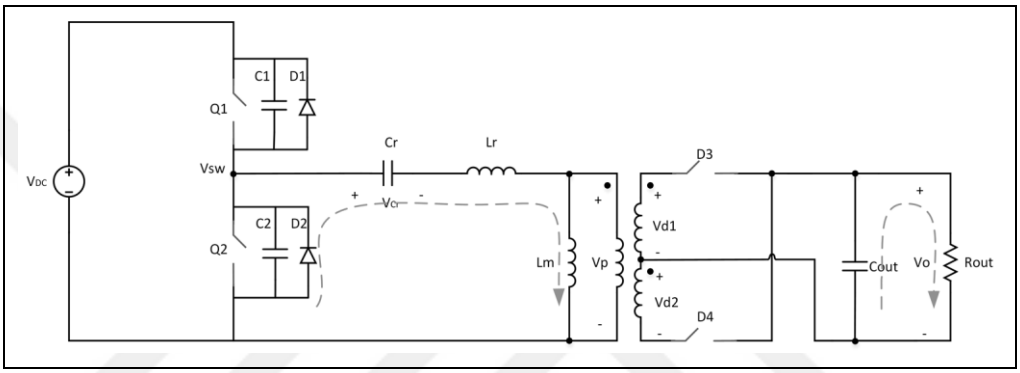

Figure 3.29: Circuit Operation for t1 to t2.

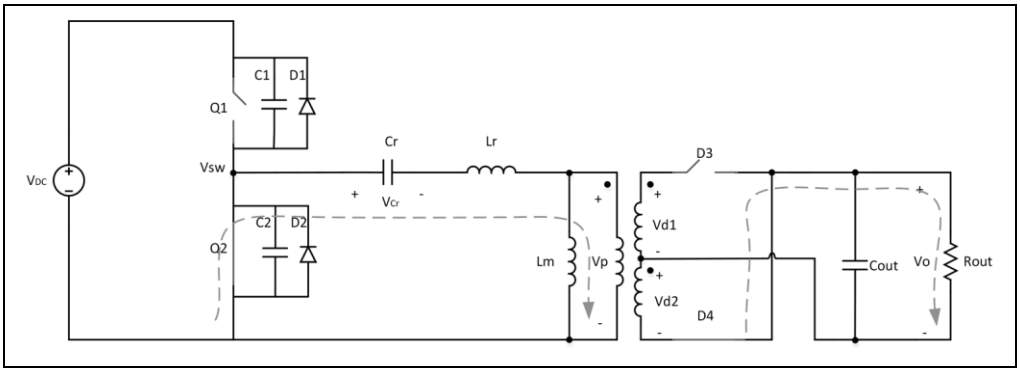

Figure 3.30: Circuit Operation for t2 to t3.

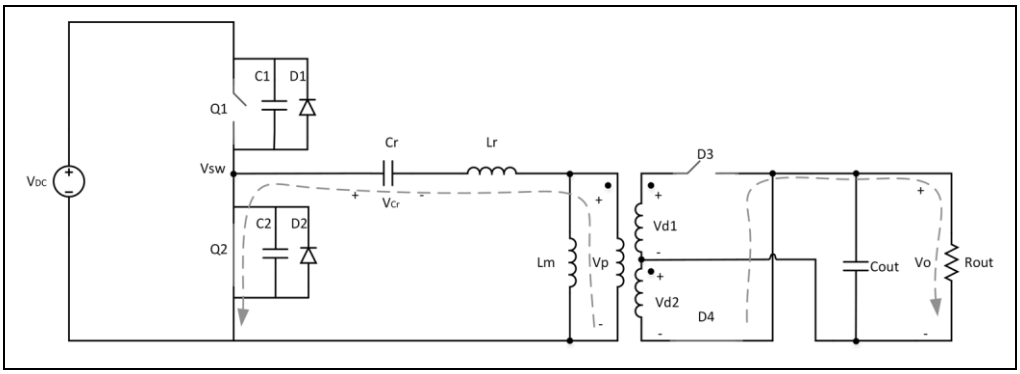

Figure 3.31: Circuit Operation for t3 to t4.

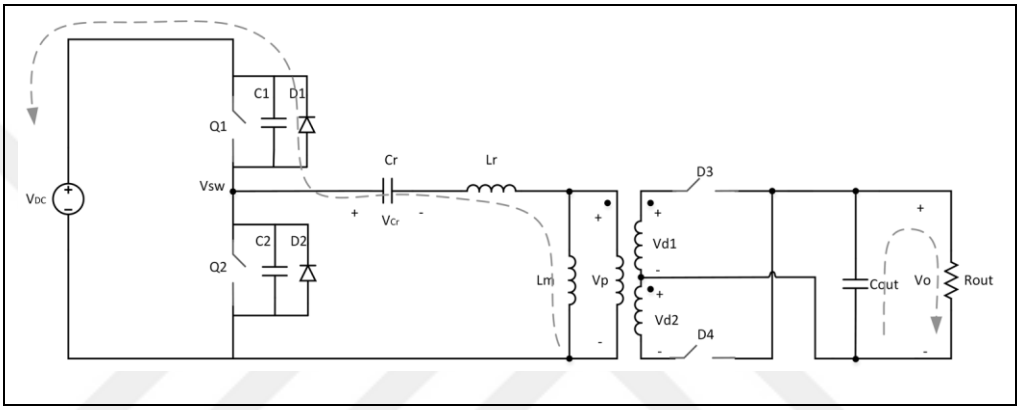

Figure 3.32: Circuit Operation for t4 to t5.

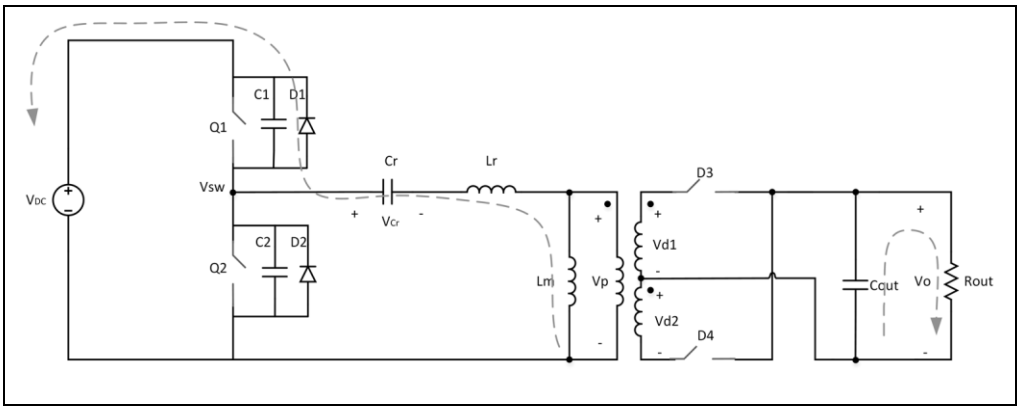

Figure 3.33: Circuit Operation for t5 to t6.

3.4.3. Operation Below Resonance

Circuit operation below resonance is valid for the switching frequency lower than the resonance frequency. In this mode, the circuit operation is similar to the

operation mode at resonance. However, some major differences change the operation dramatically at the secondary rectifier. Figure 3.34 shows the voltage and current waveforms of the primary and secondary sides. Circuit diagrams corresponding to time intervals in the waveform graph are same with operation mode at resonance and shown in from Figure 3.28 to Figure 3.33.

Because of the switching period is longer than the tank current period, I_m and I_r reach to same point before half cycle. From this point, rectifier diodes will be reverse biased due to the tank current flows only throughout magnetizing inductor.

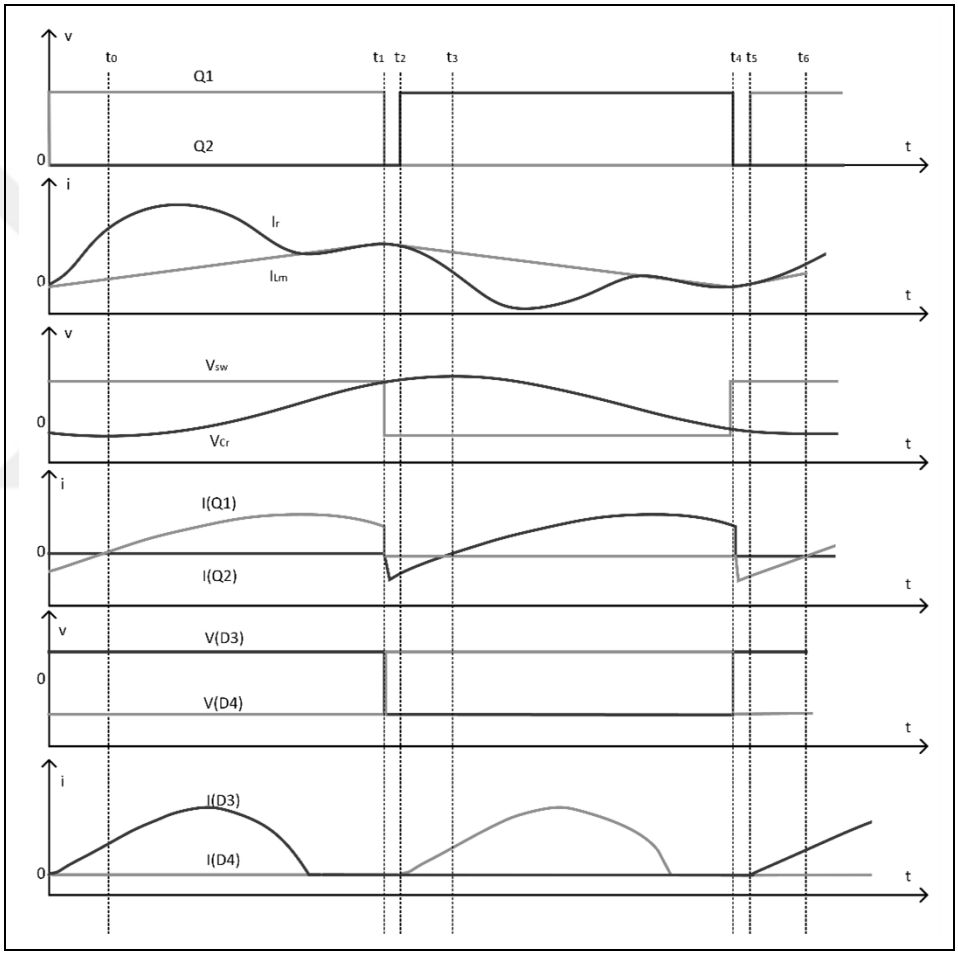

Figure 3.34: Voltage and Current Waveforms at $f_{sw}<f_r$.

3.4.4. Operation Above Resonance

Circuit operation above resonance is valid for the switching frequency higher than the resonance frequency. In this mode, the circuit operation is reversed in comparison to the operation mode at below resonance. Figure 3.35 shows the voltage

and current waveforms of the primary and secondary sides. Circuit diagrams corresponding to time intervals in the waveform graph are same with operation mode at resonance and shown in from Figure 3.28 to Figure 3.33.

Because of the switching period is shorter than the tank current period, I_m and I_r reach to same point at the start of the next half cycle. Before dead time period, I_r decays rapidly and approaches to I_m value.

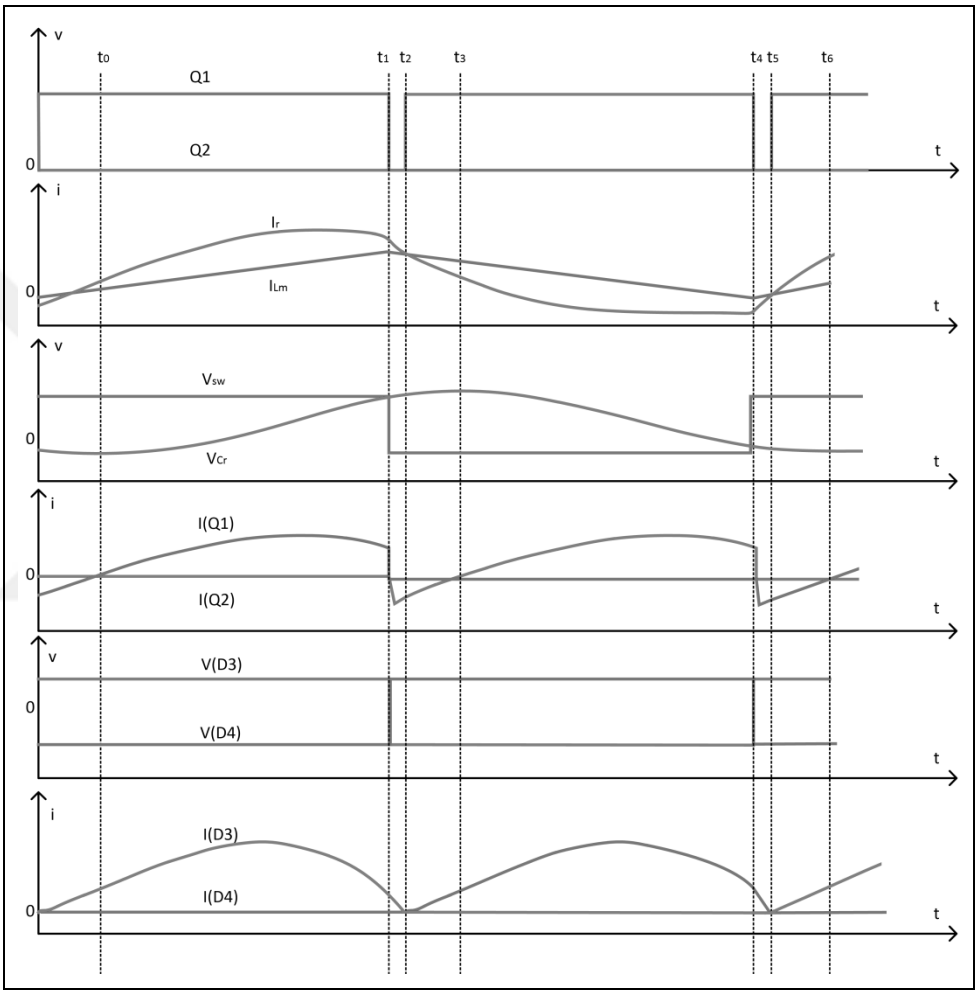

Figure 3.35: Voltage and Current Waveforms at $f_{sw}>f_r$.

3.4.5. Converter's Startup

LLC resonant converter startup sequence has importance for robustness of the converter and proper operation. In order to prevent extreme inrush currents, the output voltage is ramped up gradually and it is called as "soft start" routine.

At startup, output low pass filter acts as a short circuit for a moment. This means that the charging operation of the output capacitors must be performed in a controlled manner. This soft start routine can be implemented minimizing the energy flow to output. When the LLC resonant converter is considered, it can be provided by operation at the initial switching frequency that is much higher than the resonance frequency. It helps to reduce the converter gain and provides ZVS operation in the inductive region. As a consequence, the current is drawn from source under control by the effect of the inductive reactance of the LLC tank. After that the switching frequency is reduced in order to regulate output voltage value related to control algorithm.

4. HARDWARE DESIGN OF LLC RESONANT CONVERTER

In previous chapters, the functional blocks and operation modes of the LLC converter have been analyzed and described comprehensively. Here after a specific LLC resonant converter will be designed and design considerations will be evaluated based on the requirements as shown in Table 4.1.

Table 4.1: Design Requirements.

Requirement	**Min**	**Max**	**Unit**
Input Voltage	380	420	VDC
Output Voltage	-	24	VDC
Output Power	-	120	W
Efficiency	90	-	%
Overcurrent Capability	110	-	%

Resonant tank components will be calculated based on the analysis on the given so far and a design procedure will be followed step by step in order to meet the design specifications [Fang et al., 2013]. The design procedure is depicted as a flow diagram in Figure 4.1 and explained respectively. Before going into the details, design criteria have been defined as follows:

- The converter will operate in ZVS region in order to meet efficiency requirement.
- The converter will regulate the output voltage at light load conditions.
- For nominal input voltage, the converter will operate at resonance frequency.
- The converter must be able to handle the input voltage range.

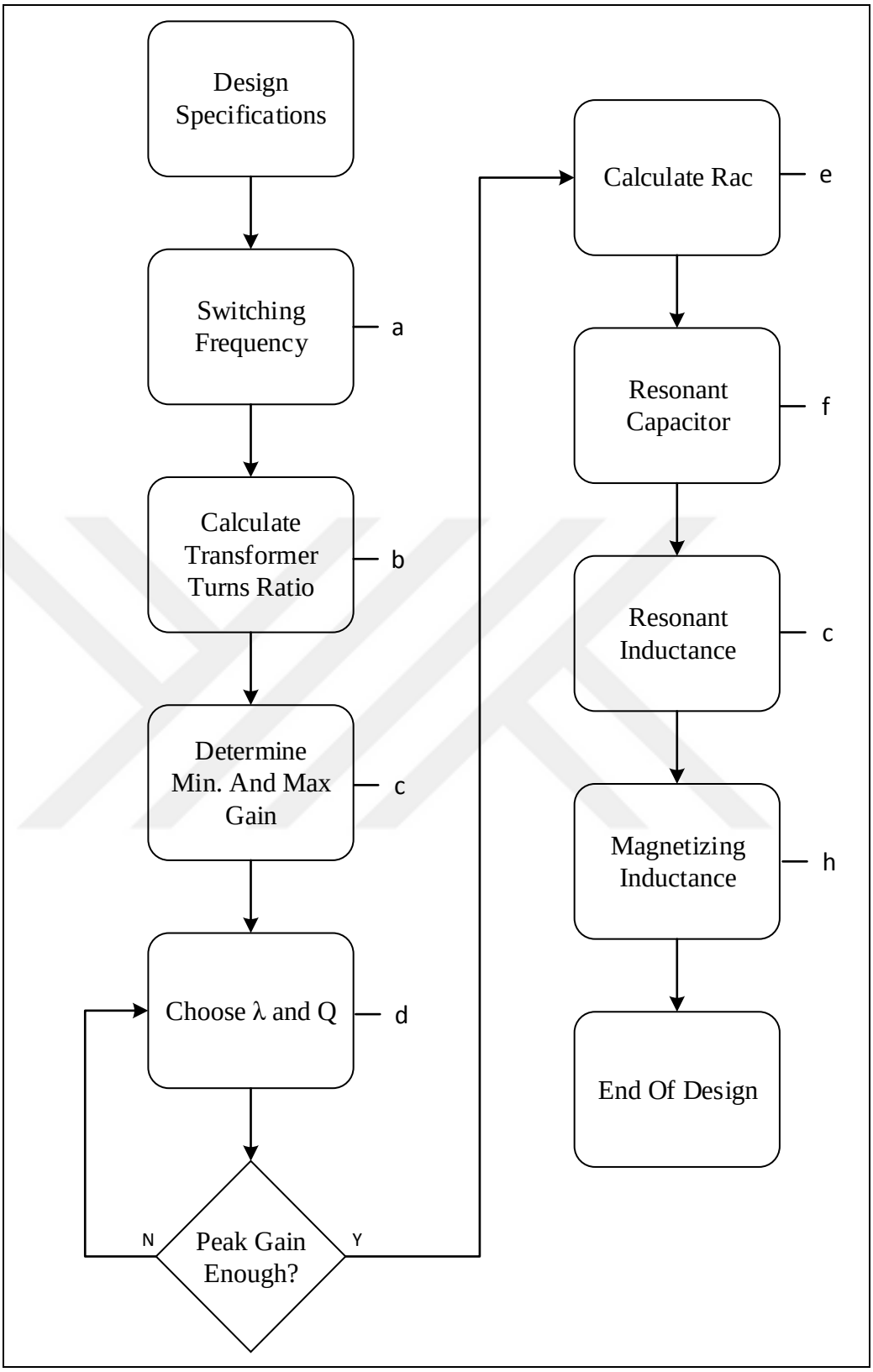

Figure 4.1: Design Procedure Flow Chart.

• Selection of the Switching Frequency

Switching frequency is one of the most important trade off in the design consideration. The higher switching frequency makes the switching losses important. In this way, the operation at the higher switching frequency benefits the advantage of ZVS efficiency of the LLC resonant converter. When the switching frequency is very high, it is necessary to take into consideration the factors such as board layout concerns, magnetic core losses, transformer stray capacitances and electronic devices availability [Buccella et al., 2012]. Additionally, EMI issues make difficult the testing process and selecting the switching frequency as lower than 150kHz is a good choice. Because for Class A and Class B devices subject to conducted EMI regulations above 150kHz according to EN55022 standard. On the other side, conduction losses become dominant at the lower switching frequency instead of the switching losses [Lu et al., 2006]. But it can cause high volume reactive components such as capacitor and transformer. In conclusion, the switching frequency range for normal operation has been selected as 70-150kHz. Also the resonance frequency has been selected 100kHz for initial of design and will be evaluated when the reactive components are calculated.

$$f_{sw} = 70 - 150kHz$$

$$f_r = 100kHz \tag{4.1}$$

• Transformer Turns Ratio

The transformer turns ratio (n) is calculated from Equation 3.33 on the assumption that the converter operates at resonance frequency for nominal input voltage:

$$n = \frac{V_{in,nom}}{2V_{o,nom}} = \frac{420}{2 \cdot 24} = 8.75 \tag{4.2}$$

• Determine Min. and Max. Gain

M_{min} and M_{max} can be determined by using Equation 3.34 and Equation 3.35, respectively:

$$M_{min} = 2n\frac{V_o}{V_{in,max}} = 2 \cdot 8.75 \cdot \frac{24}{440} = 0.95 \quad (4.3)$$

$$M_{max} = 2n\frac{V_o}{V_{in,min}} 2 \cdot 8.75 \cdot \frac{24}{360} = 1.16 \quad (4.4)$$

Secondary side rectifier diode's forward voltage and power losses have been neglected. M_{max} value is increased to 1.16*110% due to overcurrent capability in the inductive region. Thus M_{max} is obtained:

$$M_{max} = 1.16 \cdot 110\% = 1.3 \quad (4.5)$$

- Selecting Q and λ Values

Selection of Q and λ values is an iterative process based on the peak gain curves approach. Peak gain curves diagram is created by quality factor (Q) and voltage gain (M) values on the x and y axes, respectively, for fixed λ values. Maximum gain corresponding to Q values for each λ in Figure 4.2 is used to plot the peak gain curves as shown Figure 4.3.

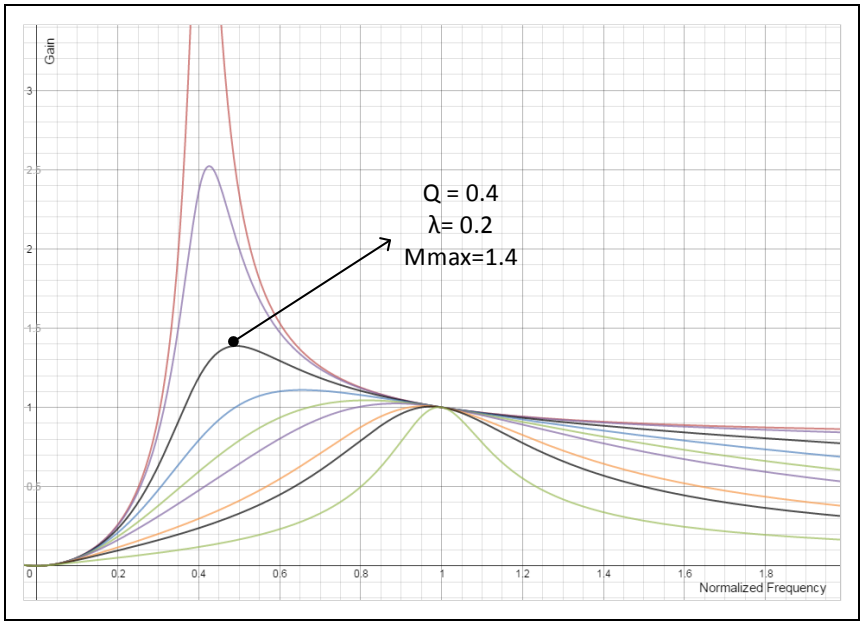

Figure 4.2: Maximum Gain for Specific Q and λ.

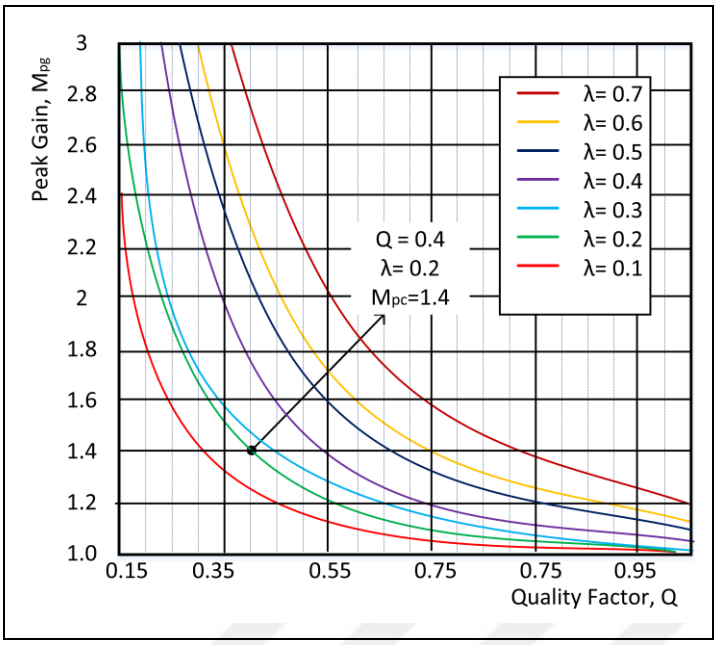

Figure 4.3: Peak Gain Curves.

Any values of M_{pg} can be selected, which are greater than 1.3 as shown in Figure 4.4. But there are many trade-offs about selection of the Q and λ when related gain value is greater than 1.3.

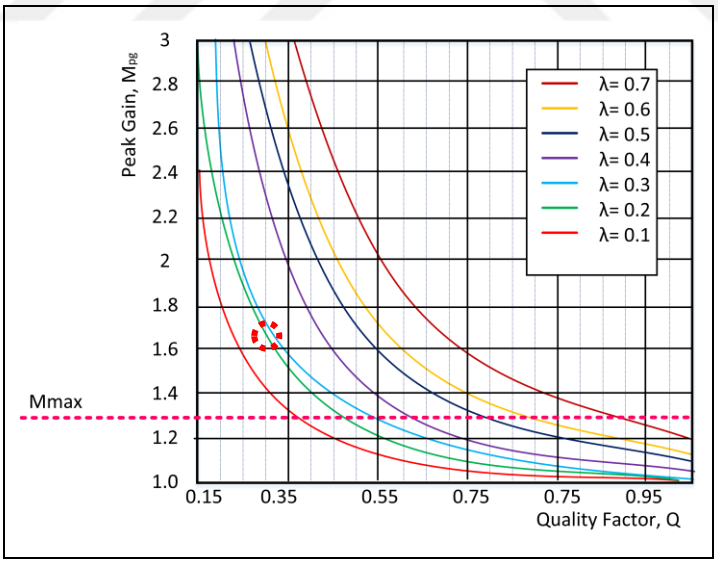

Figure 4.4: Peak Gain Curve Limit for M_{max}.

So the effects of the Q and λ can be analyzed as following:

"A smaller Ln can make the peak gain higher for a fixed Qe, keeping the design's operation out of the capacitive region. Since Ln is a ratio of the magnetizing inductance (Lm) to the series resonant inductance (Lr), a smaller Ln usually results

from a smaller Lm, and vice versa. A smaller Lm will introduce higher magnetizing current. This can help ZVS but will increase conduction losses. A smaller Qe makes the peak gain higher while associated gain curves have a larger frequency variation for a given gain adjustment. A large Qe results in a very low peak gain, which may not meet the design requirements." [TI, 2010]

In conclusion, considering all this information λ and Q have been selected as 0.2 and 0.3, respectively.

- Calculate Equivalent Load Resistance (R_{ac})

The effective load resistance reflected to primary side is calculated:

$$R_{ac} = n^2 \cdot R_e = n^2 \cdot \frac{8}{\pi^2} \cdot \frac{V_{out}}{I_{out}}$$
$$= 8.75^2 \cdot \frac{8}{\pi^2} \cdot \frac{24}{5 \cdot 110\%} = 271 \quad (4.6)$$

- Calculation of Resonant Capacitor (C_r)

The resonant capacitor can be calculated as following:

$$C_r = \frac{1}{2\pi \cdot Q \cdot f_r \cdot R_{ac}} = \frac{1}{2\pi \cdot 0.3 \cdot 100000 \cdot 271}$$
$$= 19.5nF \quad (4.7)$$

C_r is selected as 22nF due to that is the nearest standard capacitor value.

- Calculation of Resonant Inductance

The resonant inductance L_r can be calculated as following:

$$L_r = \frac{1}{(2\pi \cdot f_r)^2 \cdot C_r} = \frac{1}{(2\pi \cdot 100000)^2 \cdot 22 \cdot 10^{-9}}$$
$$= 115uH \quad (4.8)$$

The selection of L_r must be able to correspond to transformer leakage inductance value. So L_r is selected as 100uH.

- Calculation of Magnetizing Inductance

The magnetizing inductance (L_m) calculated from λ=0.2 :

$$L_m = \frac{L_r}{\lambda} = \frac{100uH}{0.2} = 500uH \quad (4.9)$$

5. SIMULATION PERFORMANCE OF CONVERTER HARDWARE

The purpose of this section is to simulate the LLC resonant converter hardware model and observe the simulation results compared to design solution. LTSpice IV tool is used in simulation phase and it uses Berkeley SPICE 3F4/5 core in order to calculate simulation results [Brocard, 2011]. Simulation process was split into in two main simulations:

- Transient Simulation : This is the transient simulation that is used for the non-linear analysis of the LLC resonant converter.
- AC Simulation : This is the dynamic simulation that is used for the analysis in frequency domain. It allows the observation of the circuit using Bode plots that provides amplitude and phase information of the converter.

The switching frequency is selected fixed 98kHz in response to 107kHz resonance frequency.

5.1. Transient Simulation

5.1.1 Simulation Model

The simulation model for analyzing transient response has been presented based on the hardware design considerations in the previously chapter as shown in Figure 5.1. The aim of this model is to verify the design parameters in order to meet design requirements of the LLC resonant converter before the real experimental design. The schematics in Figure 3.1 are used to create the converter schematics in LTSpice IV environment.

In order to execute transient simulation .tran Spice directive is used. This command provides to configure stop time, time to start saving, maximum time step and zero start attributes of the simulation.

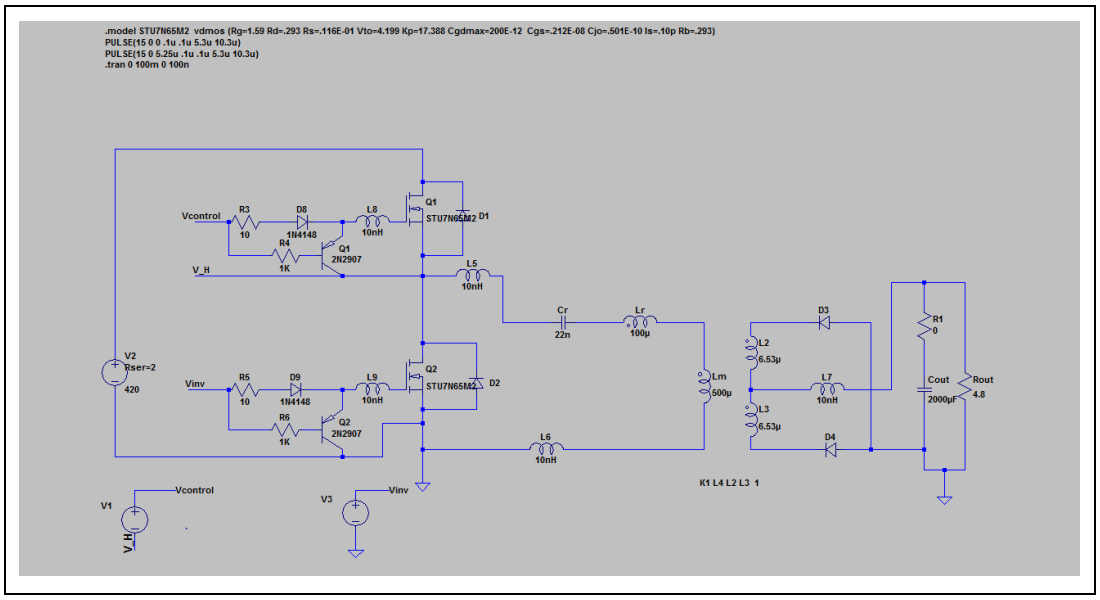

Figure 5.1: Hardware Simulation Model.

5.1.2 Simulation Results

After drawing the model and setting values of the components in the schematics, the simulation has been run.

Figure 5.2 shows output voltage (yellow), and trigger signals of the switching MOSFETs (turquoise and pink) at the initial phase of the converter.

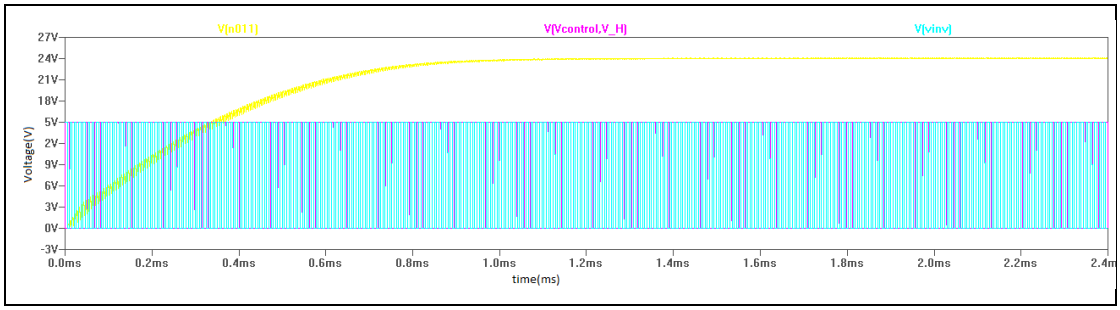

Figure 5.2: Initial Phase of Simulation.

Figure 5.3 shows the current waveforms of the MOSFETs (yellow and green) , output voltage and current (grey and blue) and trigger signals of the MOSFETs (turquoise and pink). The converter operates at 120W output load condition. From the current waveforms, it is observed that the converter operates at the near right side of the resonance frequency.

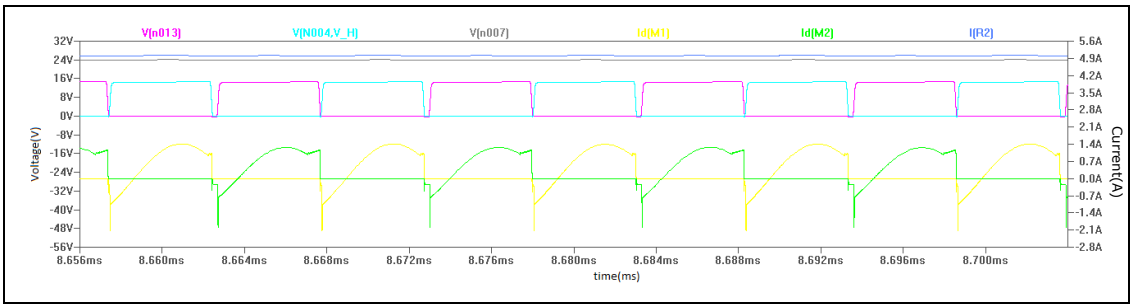

Figure 5.3: Current Waveforms of the MOSFETs.

Figure 5.4 shows the Zero Voltage Switching when the high side MOSFET Q1 turns on. When the voltage (pink) across the MOSFET decays to zero, the MOSFET trigger signal (yellow) goes to HIGH. It means that the MOSFET turns on in case of the voltage across its drain to source is zero. This operation maintains ZVS and reduces switching losses.

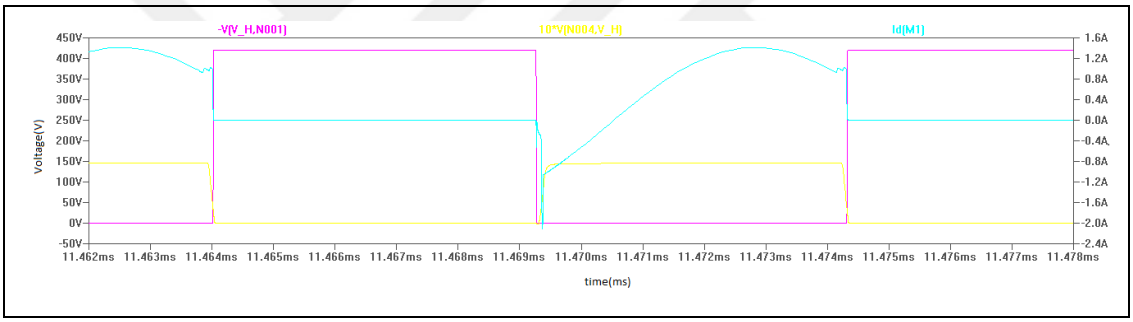

Figure 5.4: ZVS for Q1 MOSFET.

Resonant tank current (red) and resonant capacitor voltage (yellow) can be seen from Figure 5.5. The operation region of the resonant tank is inductive and the current lags behind the voltage, so that providing ZVS operation.

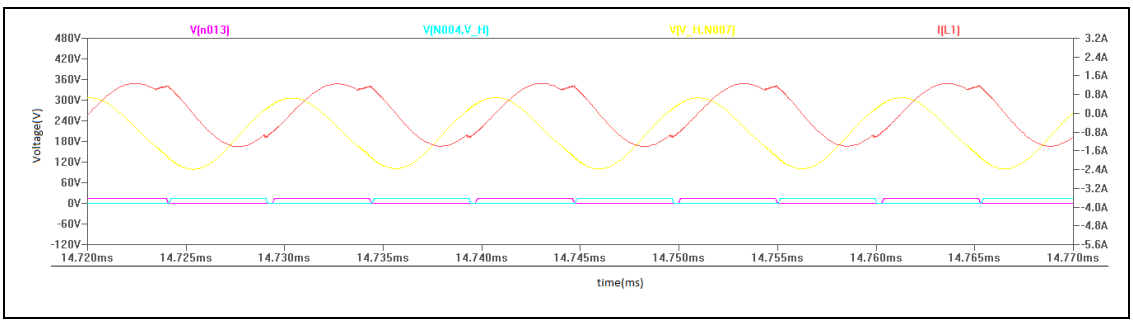

Figure 5.5: Resonant Tank Current and Resonant Capacitor Voltage.

Secondary side diode D3 voltage (red) is depicted in Figure 5.6. The voltage across the diode anode-cathode is 2*Vout and forward biased in accordance with Q1 trigger signal (pink).

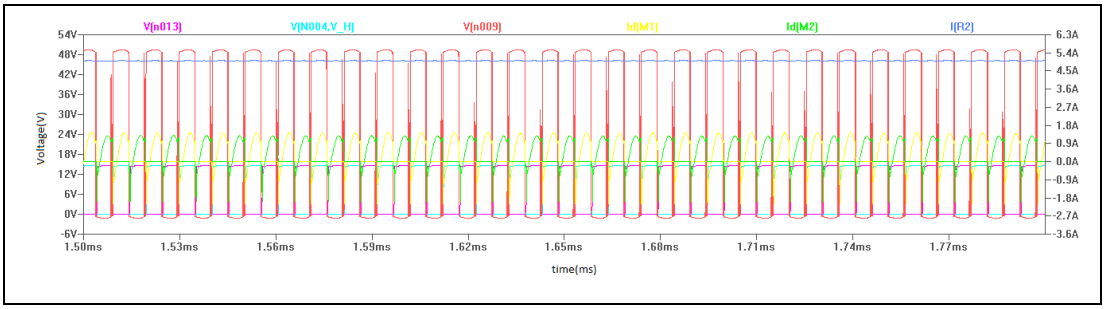

Figure 5.6: Secondary Rectifier Diode (D3) Voltage.

5.2. AC Simulation

5.2.1 Simulation Model

In order to implement AC simulation of the LLC resonant converter, FHA model has been created in the simulation environment as shown in Figure 5.7. The simulation is made for various equivalent resistors. Therefore, .step spice directive is used to sweep for different resistance values.

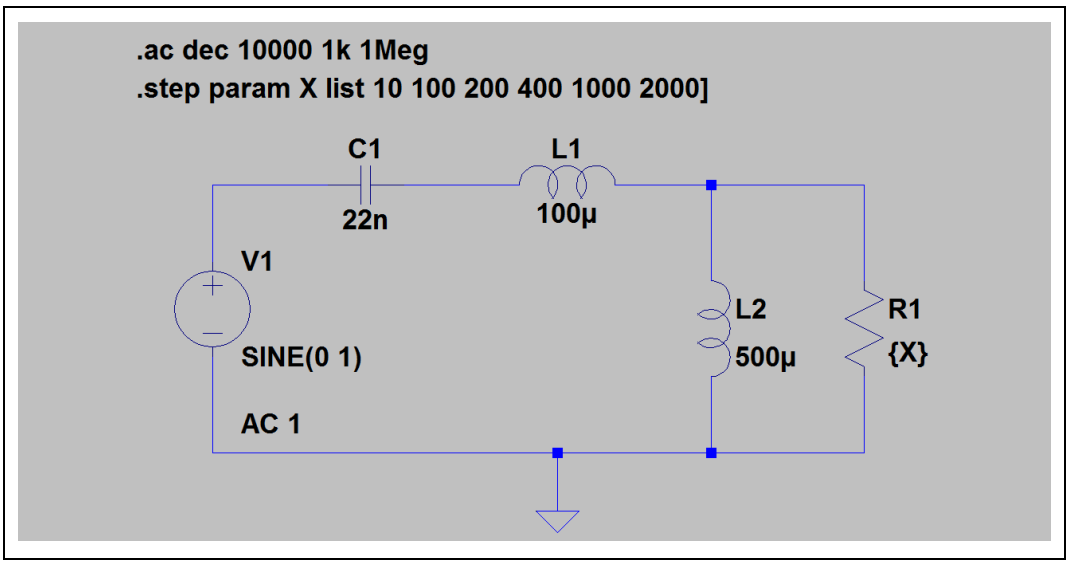

Figure 5.7: FHA Simulation Model.

5.2.2 Simulation Results

The frequency response of the LLC converter output voltage is obtained as bode plot in Figure 5.8. The top pane shows the phase and the bottom pane shows the magnitude response of the converter. For all load conditions, the converter has unity gain at 107kHz that is the resonance frequency. It is clear that the output voltage is in phase at the resonating point.

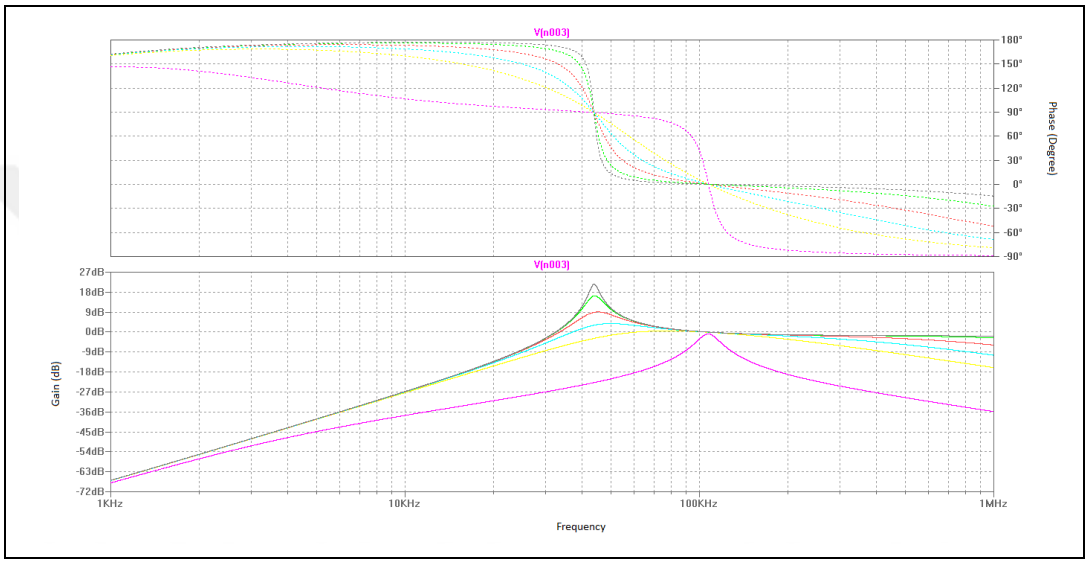

Figure 5.8: Bode Plot Diagram.

6. DESIGN OF DIGITAL CONTROLLER

Applying digital techniques to the control of DC-DC converters presents improved performance, lower costs and product flexibility. Implementing the power converter operation characteristic with embedded software instead of discrete electronic components offers space and cost savings, and robust control algorithms [Geof Potter, 2004]. Digital control is applied to feedback mechanism that regulates the output voltage and peripheral functions such as temperature control and serial communication.

In this chapter a typical digital control system is first discussed. A PID feedback controller principle is presented and PID parameters are designed in order to control LLC resonant converter properly.

Many microcontrollers and DSPs include high resolution PWM module and analog-to-digital converters. As mentioned before, it allows the software based implementation of the controller functions. A generalized digital control system that is taken from Corradini's digital control book is depicted in Figure 6.1.

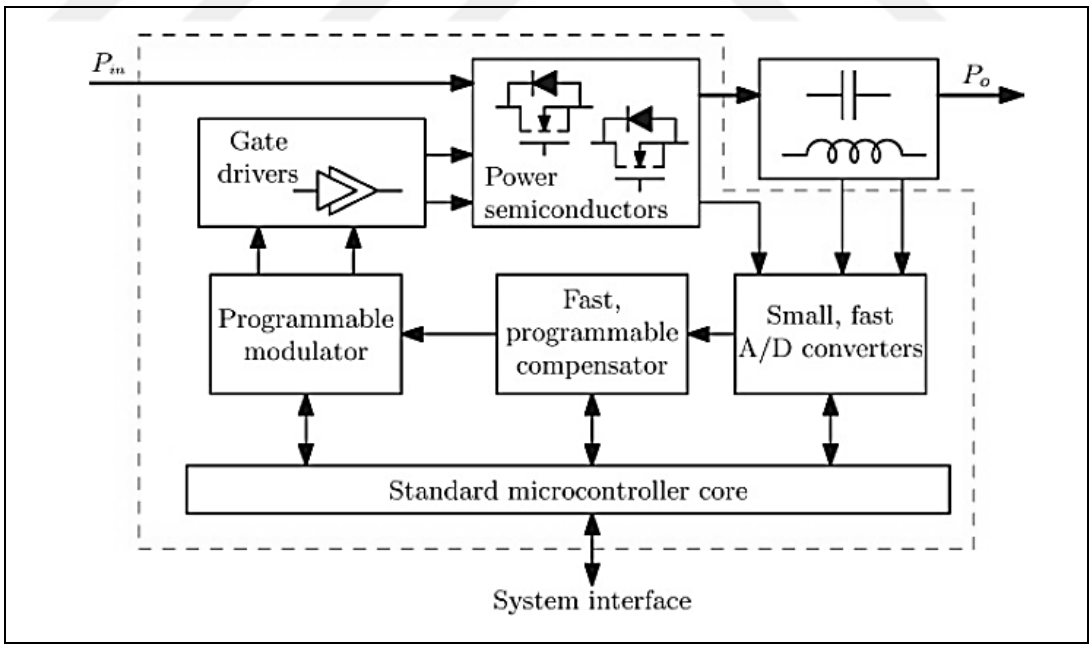

Figure 6.1: Digital Controller Architecture for LLC Resonant Converter.

6.1. PID Controller

A proportional-integral-derivative controller (PID controller) is widely used as a control loop feedback mechanism in industry. A PID controller efforts to correct the error between a set point and actual measured process variable by calculating and then outputting a corrective action that can eliminate the error.

The PID controller performs based on three separate parameters; the Proportional, the Integral and the Derivative values. The Proportional, the Integral and the Derivative parameters determine the reaction to the current error, based on the sum of recent errors and to the rate at which the error has been changing, respectively. The weighted sum of the effects of the PID parameters is used to adjust process variable. By tuning the three parameters can provide proper control action depends on the process type.

The controller output can be written as

$$V_m(t) = P_{out} + I_{out} + D_{out} \tag{6.1}$$

where P_{out}, I_{out} and D_{out} are the outputs of each of the parameters. The three outputs can be expressed as

$$P_{out} = K_p e(t) \tag{6.2}$$

$$I_{out} = K_i \int_0^t e(t) \tag{6.3}$$

$$D_{out} = K_d \frac{d}{dt} e(t) \tag{6.4}$$

The final form of the overall controller output is

$$V_m(t) = K_p e(t) + K_i \int_0^t e(t) + K_d \frac{d}{dt} e(t) \tag{6.5}$$

6.2. PID Controller Tuning

Tuning a PID controller is adjustment of the K_p, K_i and K_d parameters in order to produce output steadily. So if the parameters are chosen incorrectly, the output of the controller will be unstable.

There are three main tuning methods for a closed loop PID controller as shown in Table 6.1 [Web 1, 2015].

Table 6.1: Typical Methods for Tuning PID Controller.

Method	Advantages	Disadvantages
Manual	No math required; online options available	Requires experience in control tuning
Ziegler-Nichols	Proven method; online options available	Some process upsetting involved; can be a very aggressive tuning method
Software	Consistent tuning options available	Acquisition costs of software (such as MATLAB) can be prohibitive for some organizations; software training required

Before selection of the tuning method, Kp, Ki and Kd parameters' effects on the controller output must be known. Table 6.2 shows the effects of the parameters by the means of rise time, overshoot, resolving time, steady state error and system stability [Web 1, 2015].

Table 6.2: Effects of the PID Parameters on Controller Output.

Variable	Rise Time	Overshoot	Resolving Time	Steady State Error	System Stability
Increase K_p	Decrease	Increase	Small Decrease	Decrease	Decrease
Increase K_i	Small Decrease	Increase	Increase	Large Increase	Decrease
Increase K_d	Small Decrease	Decrease	Decrease	Minor Effect	Increase
Decrease K_p	Increase	Decrease	Small Increase	Increase	Increase
Decrease K_i	Small Decrease	Decrease	Decrease	Increase	Increase

6.2.1. PID Controller Tuning of LLC Resonant Converter

First of all, the derivative term (K_d) of the controller is not used for the LLC resonant converter control implementation. Because differentiation of a signal amplifies noise. So the derivative term is susceptible to noise in the error signal and can cause the controller output is unstable. In conclusion, a PI controller will be tuned for the feedback controller of the LLC resonant converter.

Tuning method is selected as manual tuning because of its simplicity and the simulations of the PID controller are carried out in MATLAB® Simulink.

Manual tuning process is as follows:

- Set K_p, K_i and K_d to zero.
- Increase K_p term until the control loop begins to oscillate.
- Reduce K_p to one-half of this value to obtain a quarter wave decay.
- Increase K_i term to adjust the behavior of the steady state offset.

MATLAB® Simulink model of the converter is shown in Figure 6.2. When the tuning procedure is implemented to model, the control loop has started to oscillate at K_p=3.5. K_p and K_i are calculated 1.75 and 600, respectively.

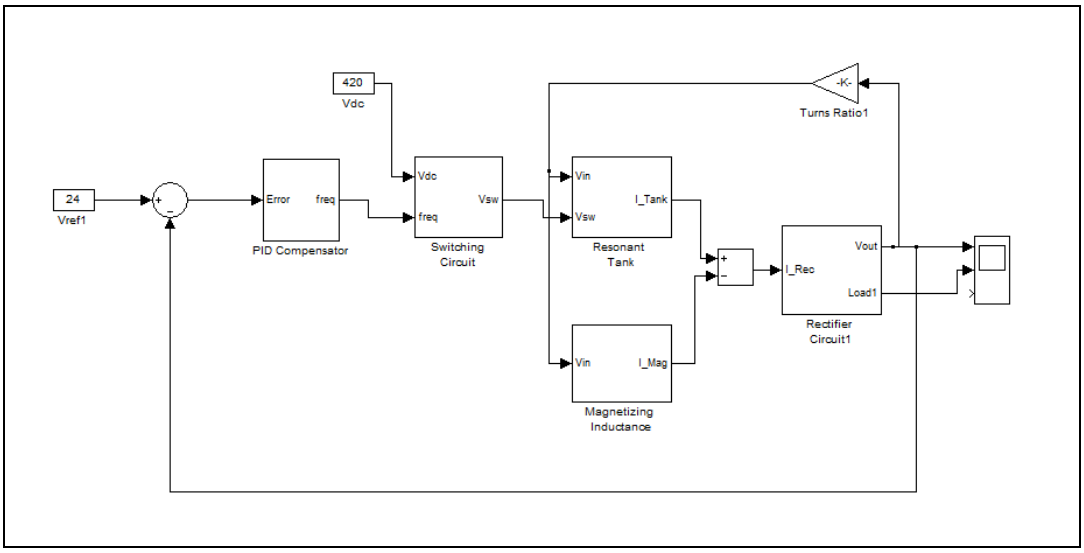

Figure 6.2: MATLAB® Simulink Model of the Converter.

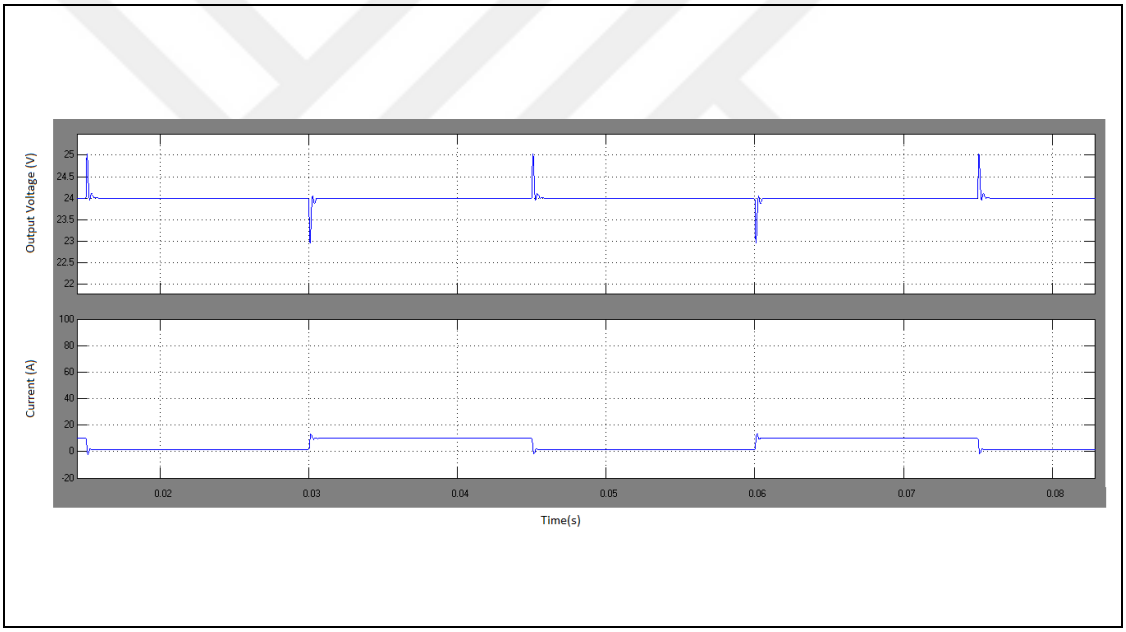

Figure 6.3: Dynamic Load Response and Steady State Error.

6.3. Implementation of Digital Controller

The main aim of the digital controller is regulation of the output voltage of the LLC resonant converter. Additionally, the main tasks of the digital controller include:

- Performing digital controller,

- Provide the gate signals for the power MOSFETs,
- Control of the interface circuits.

To implement the closed voltage control loop digitally, a DSP controller is required. In this thesis, ARM® Cortex®-M4 32 bit STM32F429 MCU was selected as digital signal processor as it has the great features in order to control a DC-DC converter such as 180MHz clock frequency, 12-bit and 7.2 MSPS ADC, 32-bit timers and floating point unit. Figure 6.4 shows the architecture of the STM32F429 MCU in the STM32F4xx datasheet from ST.

The ARM® Cortex®-M4 supports 32-bit RISC processor that provides the code efficiency and the processor supports DSP instructions that feature efficient signal processing and execution of complex algorithms.

The MCU has embedded flash memory of 2Mbytes for program and data storing. Additionally, it has 256Kbytes of SRAM that includes 64Kbytes of core coupled memory and 4 Kbytes of SRAM for backup. This memory is only accessible from the CPU.

The device includes two general purpose DMAs that provide the management of memory to peripheral, peripheral to memory and memory to memory transfers.

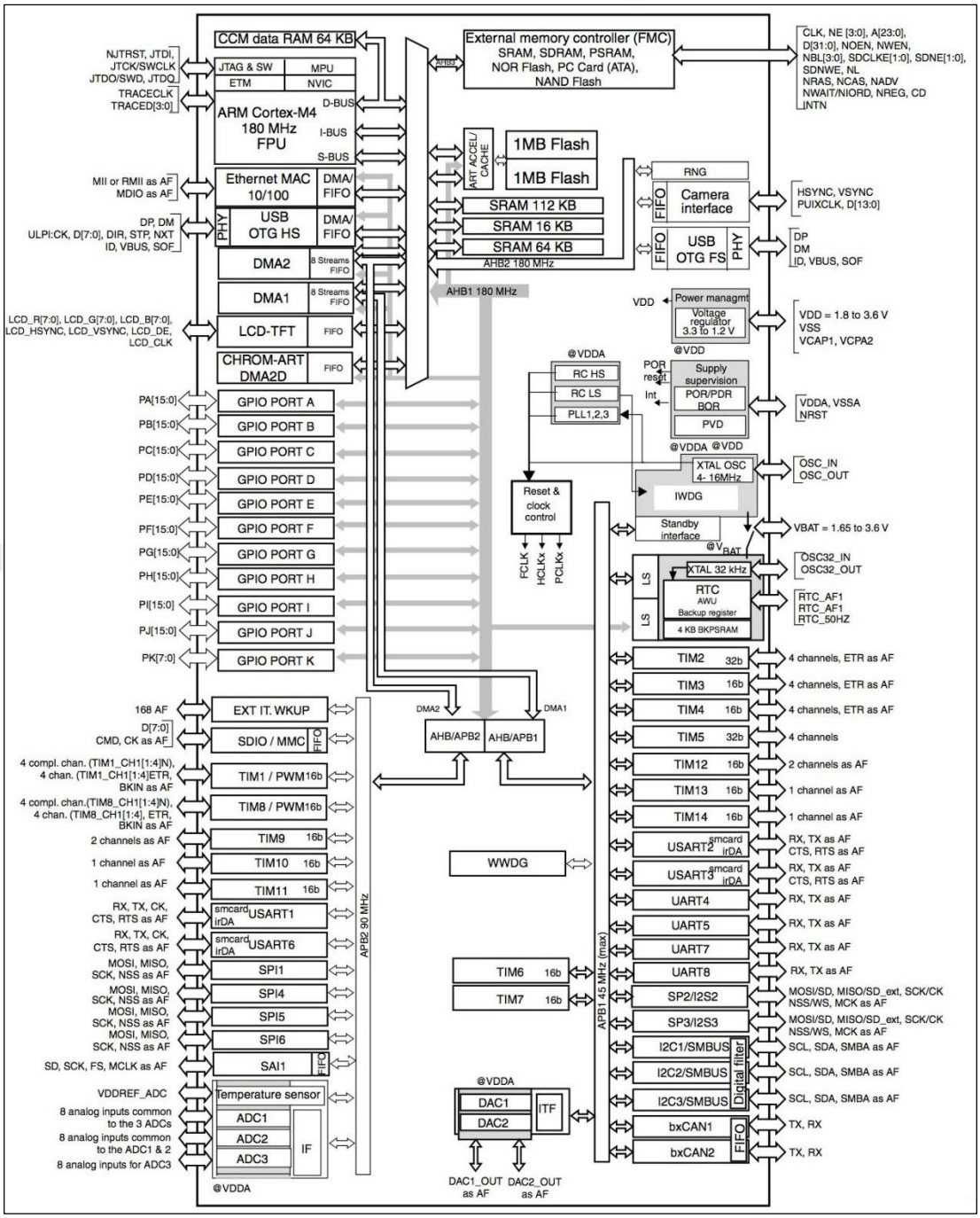

Figure 6.4: STM32F429 Block Diagram.

6.3.1. PWM Generators and ADC of STM32F429

PWM and ADC peripherals are the most important modules of the MCU. Their performances affect directly the operation of the converter. STM32F429 provides high performance and accuracy ADC and advanced PWM generators that provides the controller requirements.

32-bit Timer1 is used as PWM generators in order to drive gate signals of the power MOSFETs.

6.3.2. Digital Controller Block Scheme

Digital controller implementation using STM32F429 MCU is illustrated in Figure 6.5. Isolation between MCU and power MOSFETs is provided by optocoupler gate drivers.

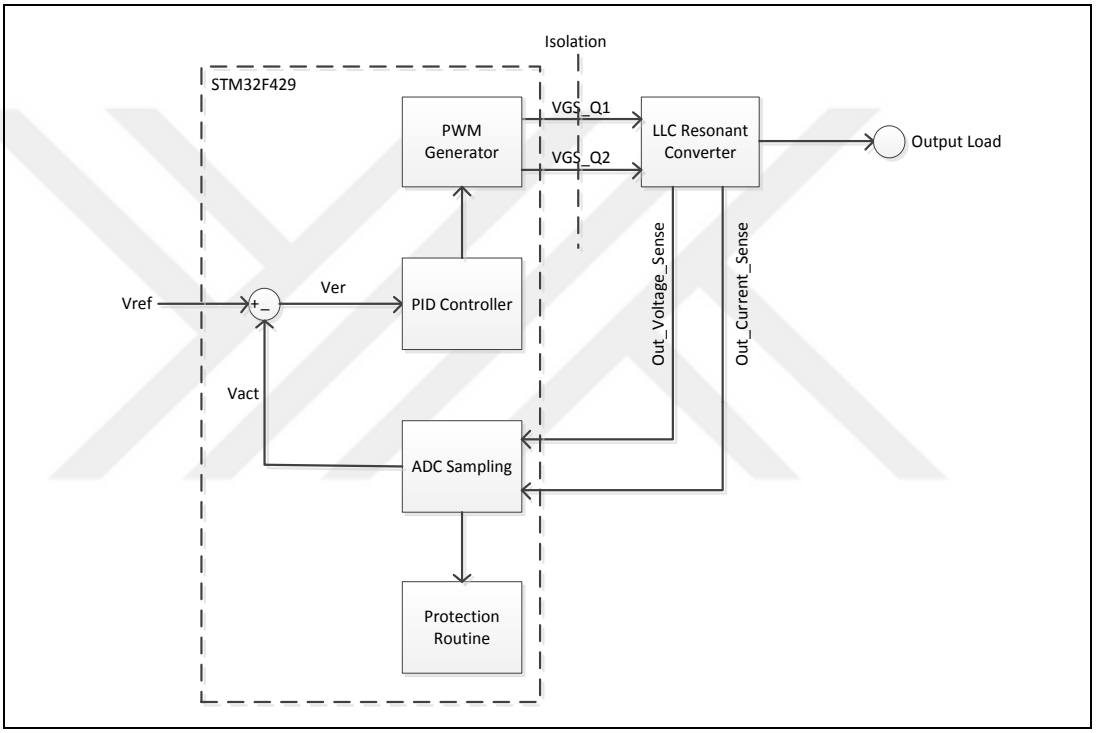

Figure 6.5: Digital Controller Block Scheme.

6.3.3. Digital Controller Algorithm

Digital controller algorithm is developed using C language in Keil uVision Development environment. The flow chart of the algorithm is depicted in Figure 6.6.

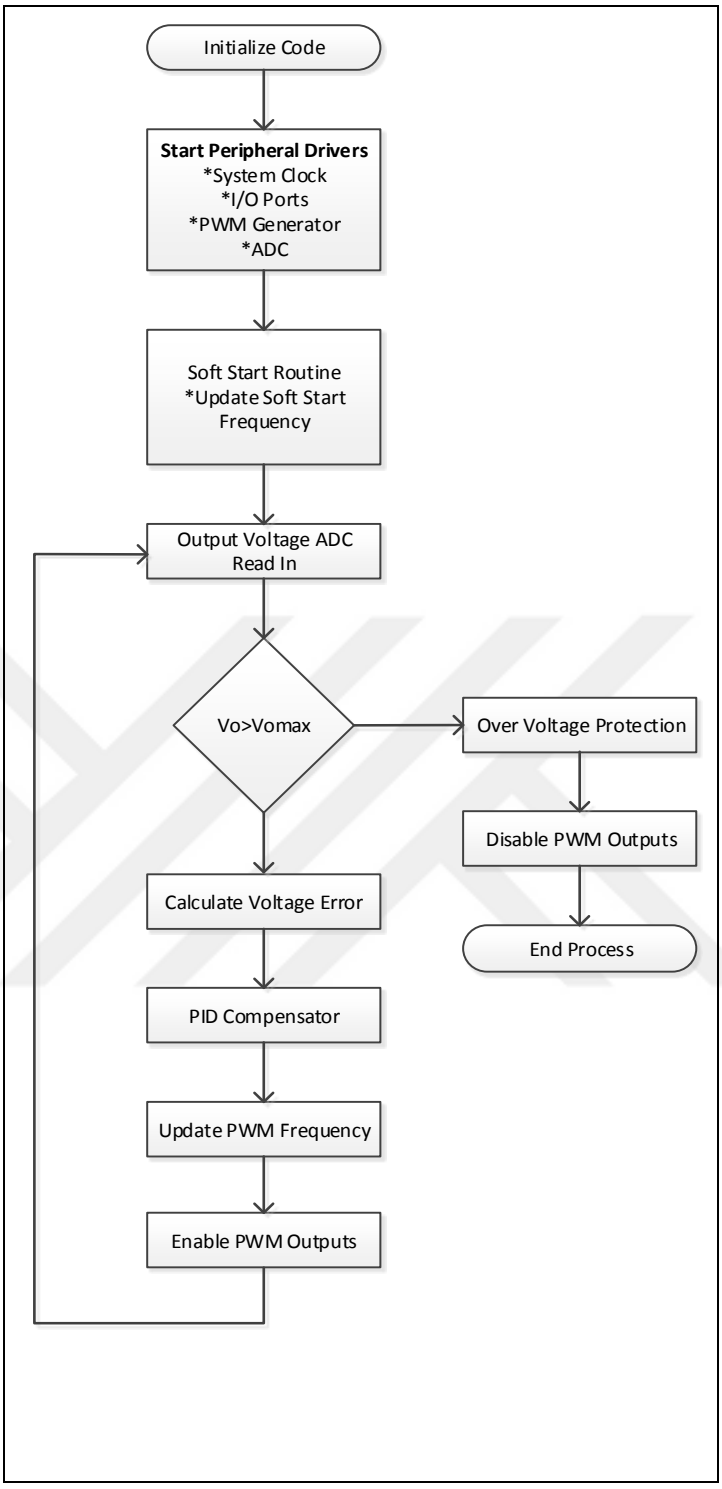

Figure 6.6: Flow Chart of the Digital Controller Algorithm.

7. EXPERIMENTAL RESULTS

7.1. Schematics and PCB Layout Design

LLC half-bridge resonant converter schematics and PCB layout are designed in accordance with calculations and simulations in Altium Designer® environment as shown in Figure 7.1 through Figure 7.7.

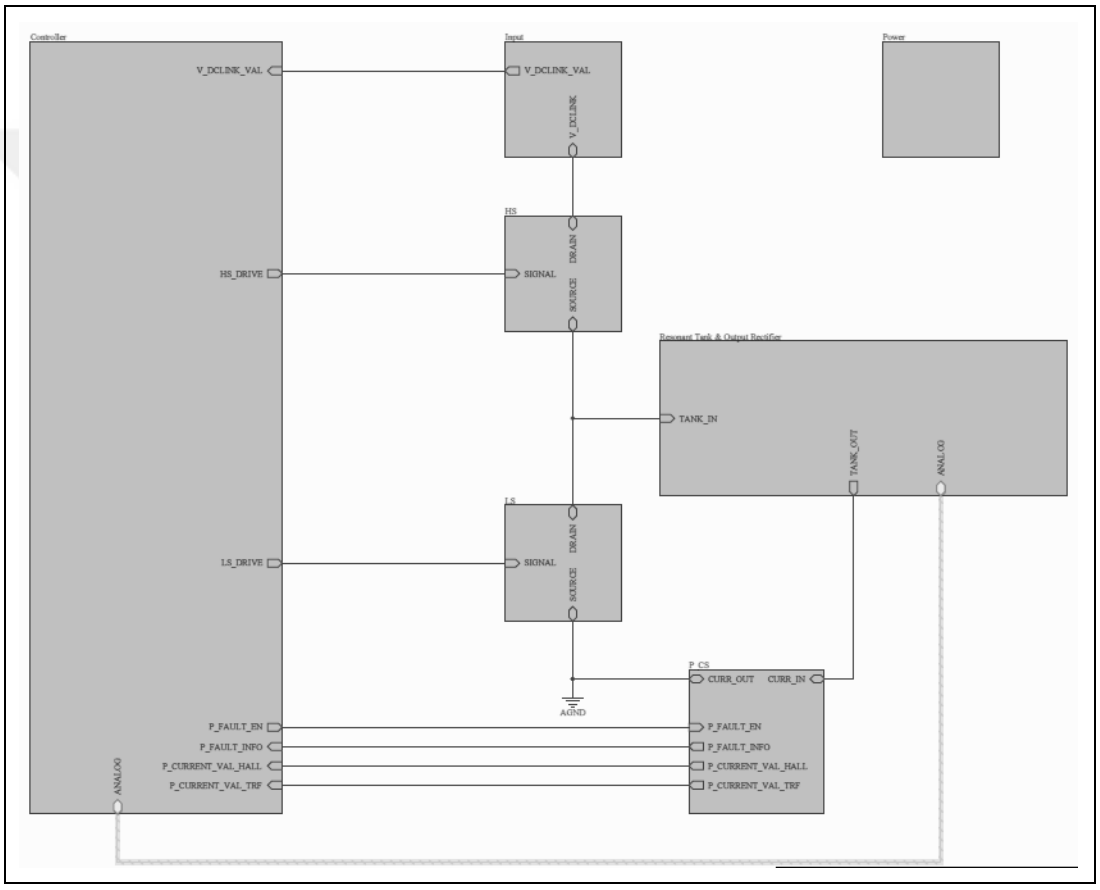

Figure 7.1: General Block Diagram of the Schematics.

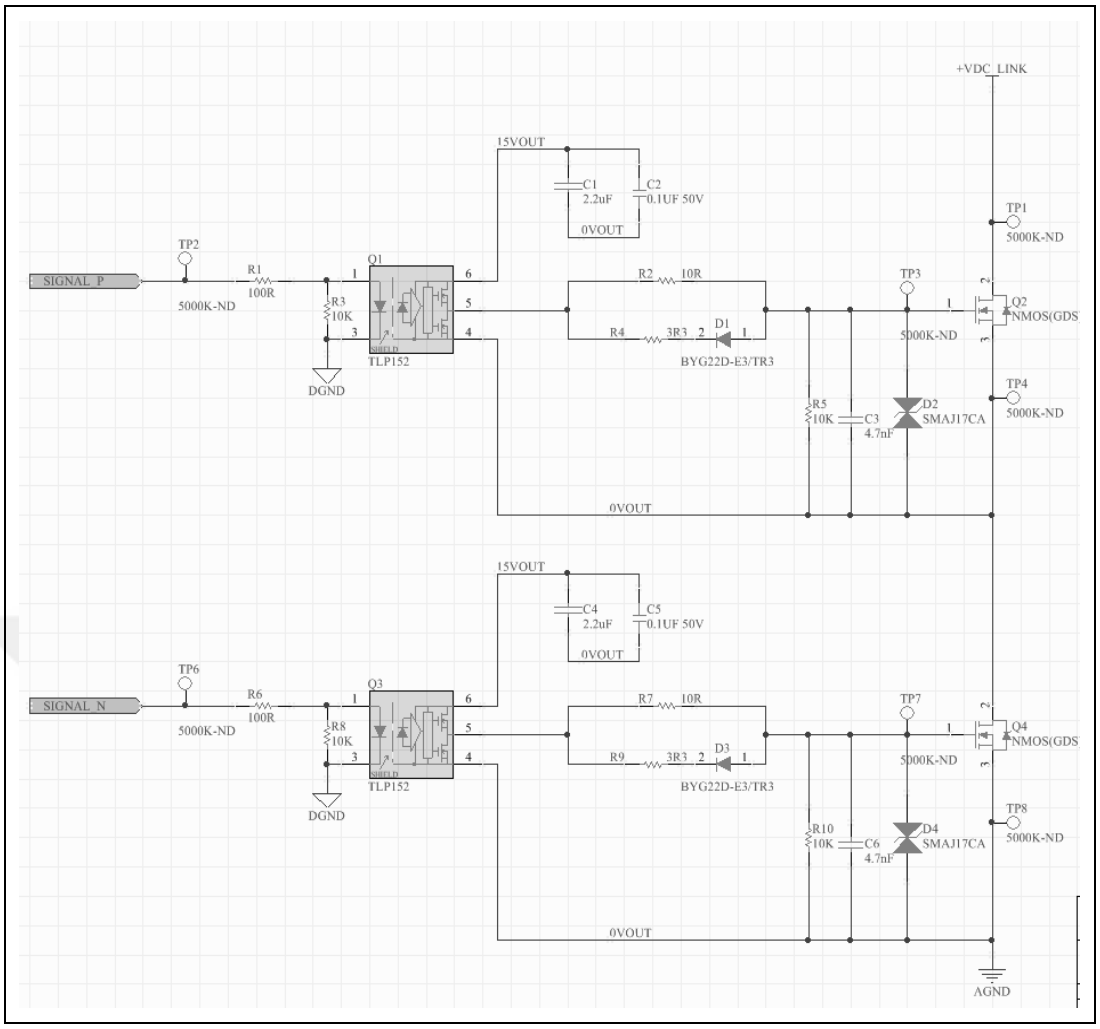

Figure 7.2: Half Bridge Structure and Drivers.

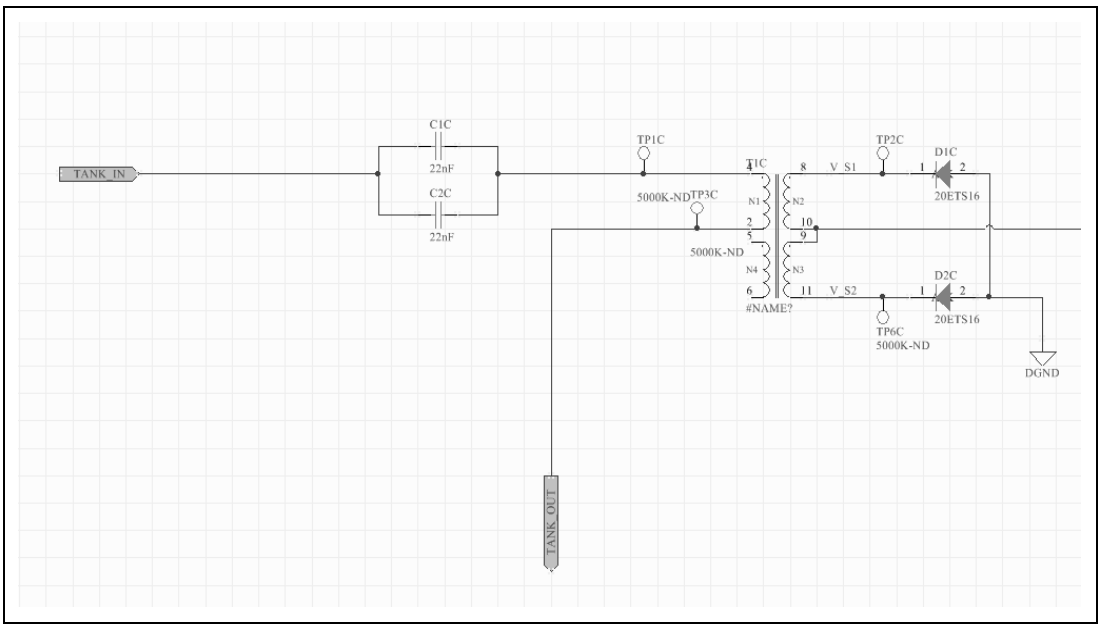

Figure 7.3: Resonant Tank and Secondary Rectifier.

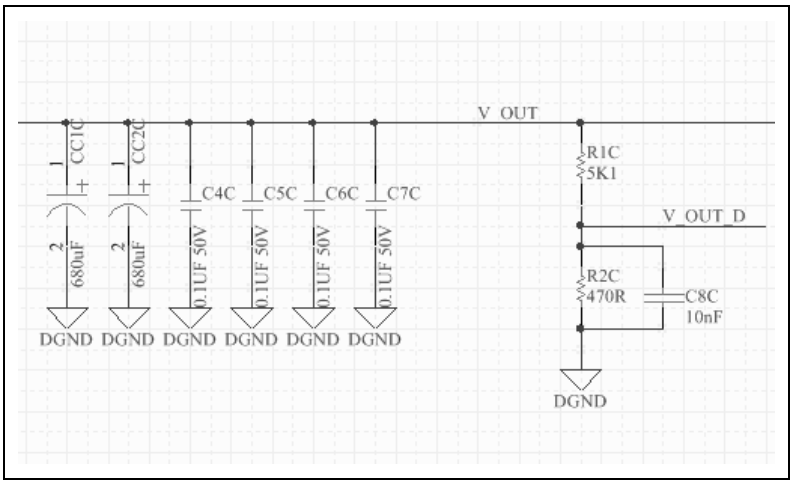

Figure 7.4: Low Pass Filter and Voltage Sense.

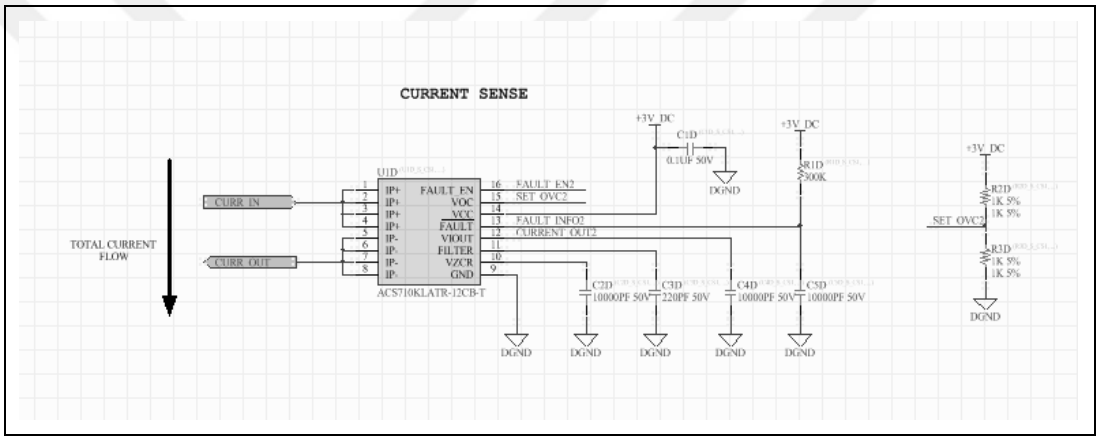

Figure 7.5: Current Sense.

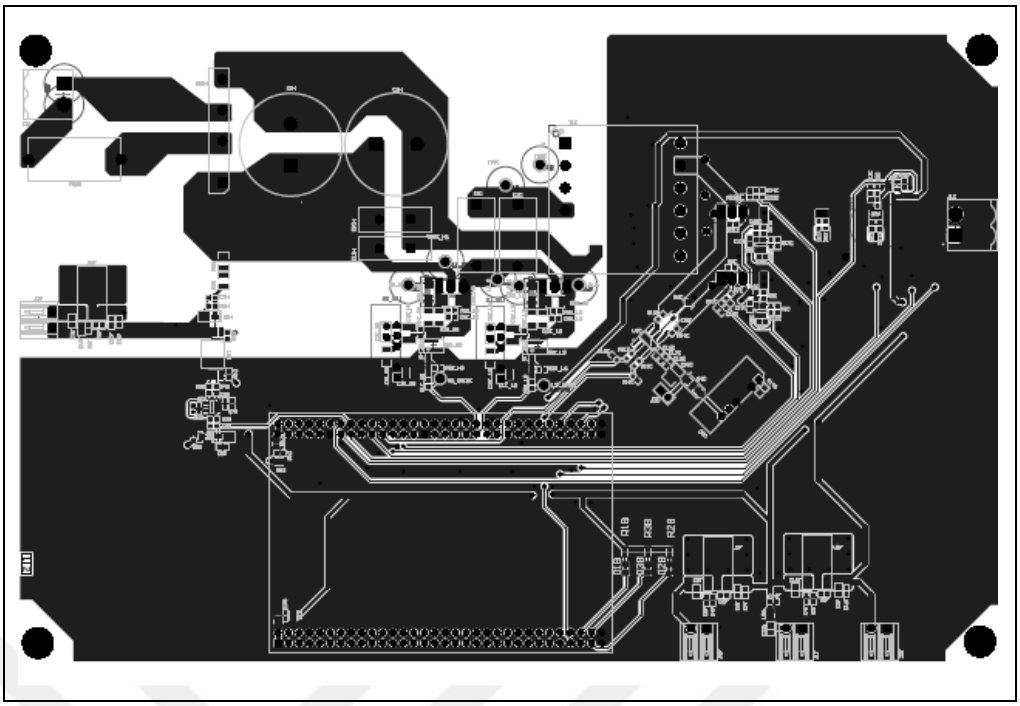

Figure 7.6: Top PCB Layout.

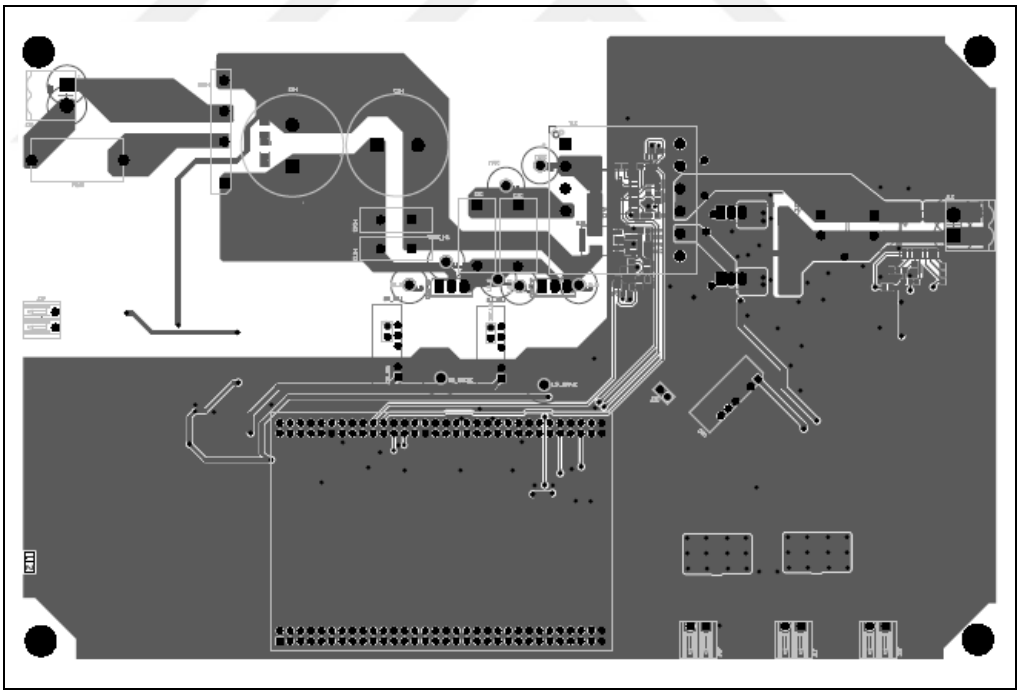

Figure 7.7: Bottom PCB Layout.

Final design board has been assembled as shown in Figure 7.8.

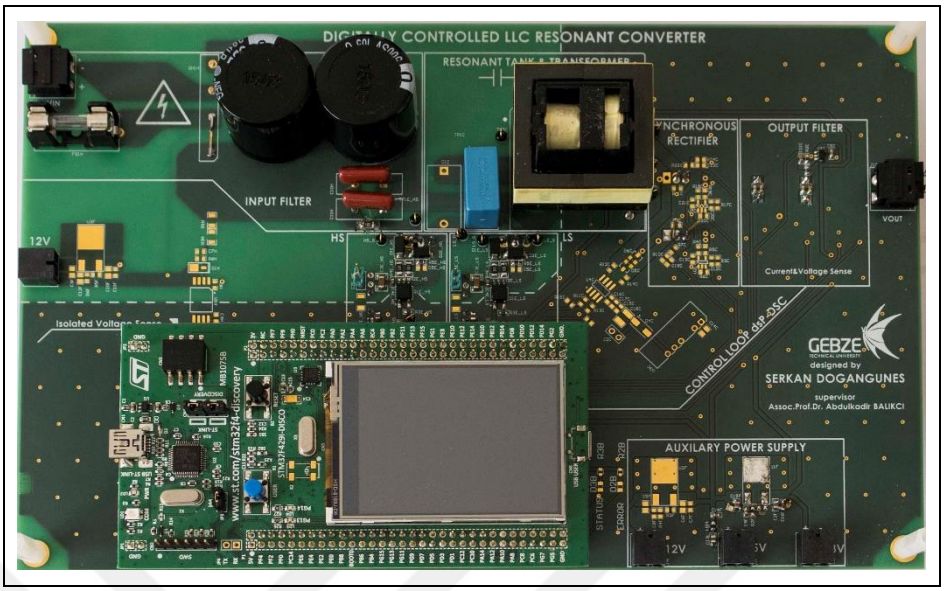

Figure 7.8: Assembled Printed Circuit Board View.

7.2. Experimental Setup

In order to verify the proposed system, some experiments are carried out. Figure 7.4 shows the experimental setup for the 120W LLC resonant converter design verification. The setup consists of the following:

- LLC Half Bridge Resonant Converter : Proposed Design
- PFC Board: 390VDC Supply
- Auxiliary Power Supply
- 120W Load

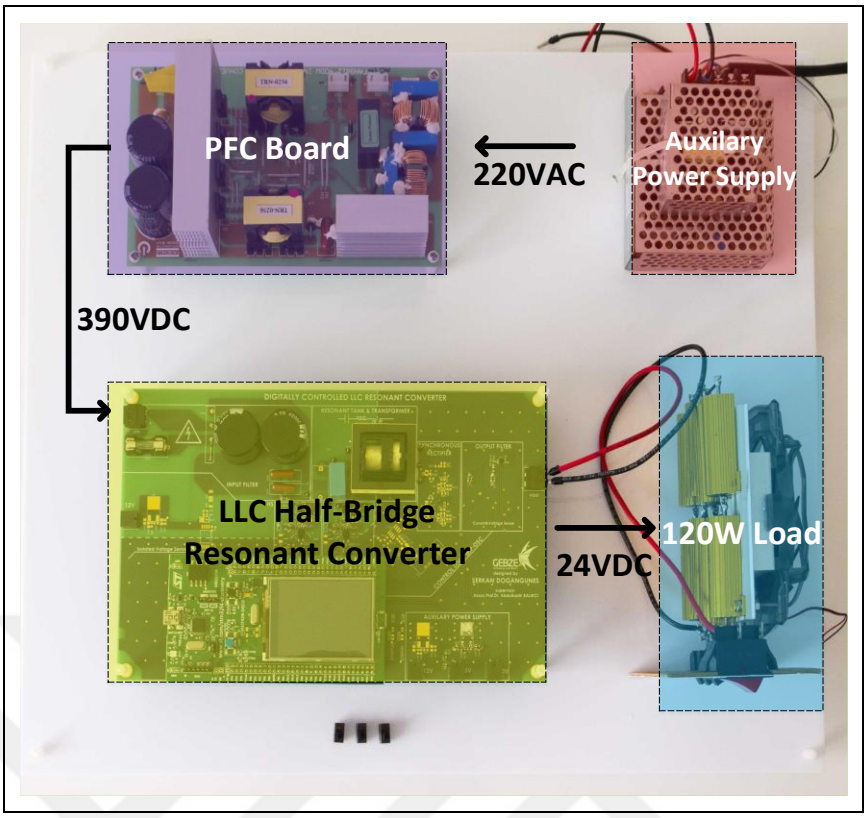

Figure 7.9: Experimental Setup.

7.3. Electrical Test Results and Operational Waveforms

In this chapter, the report of the test results is presented. Operational waveforms are captured using Tektronix TPS2024B isolated oscilloscope.

7.3.1. Soft Start Operation

The initial phase of the converter is depicted in Figure 7.10. The controller starts to drive the MOSFETs with a 250kHz PWM signal. At the end of the soft start period, output voltage is regulated at 24VDC.

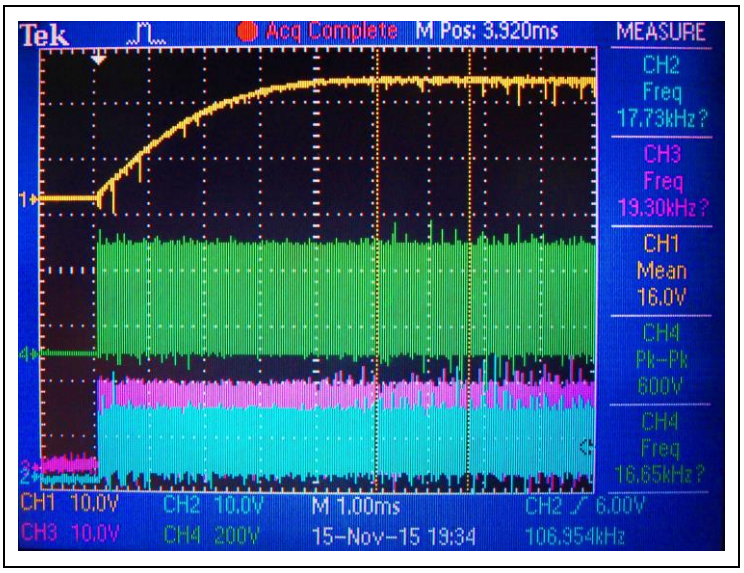

Figure 7.10: Soft Start Operation.

- Channel 1 : Output Voltage
- Channel 2 : Gate to Source Voltage of the MOSFET Q1
- Channel 3 : Gate to Source Voltage of the MOSFET Q2
- Channel 4 : Vsw (Half Bridge Voltage)

7.3.2. Dynamic Load Response

Dynamic load response is demonstrated in Figure 7.11 during load transitions which are full load to no load, and vice versa. Overshoot and undershoot are measured as 1.5V.

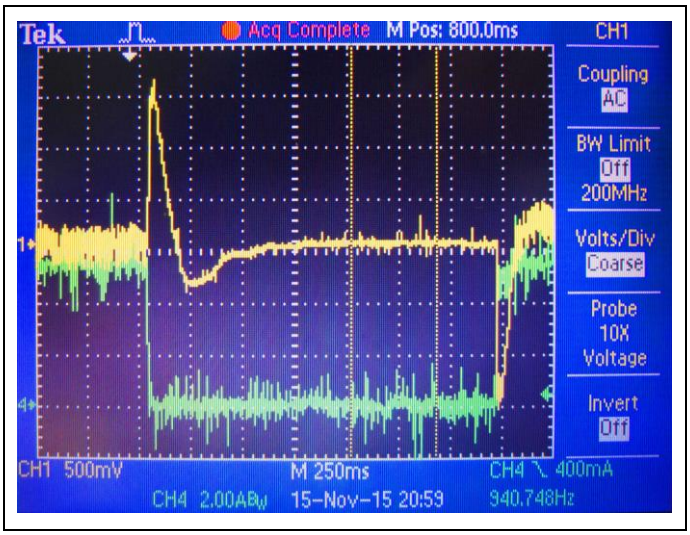

Figure 7.11: Dynamic Load Response.

- Channel 1 : Output Voltage
- Channel 4 : Output Current

7.3.3. Output Voltage Ripple

Output voltage ripple is measured 50mV at full load condition. The spikes on the waveform are neglected because the measurement of the high switching voltage affects the output voltage ripple. It is verified with measurement using Fluke multimeter.

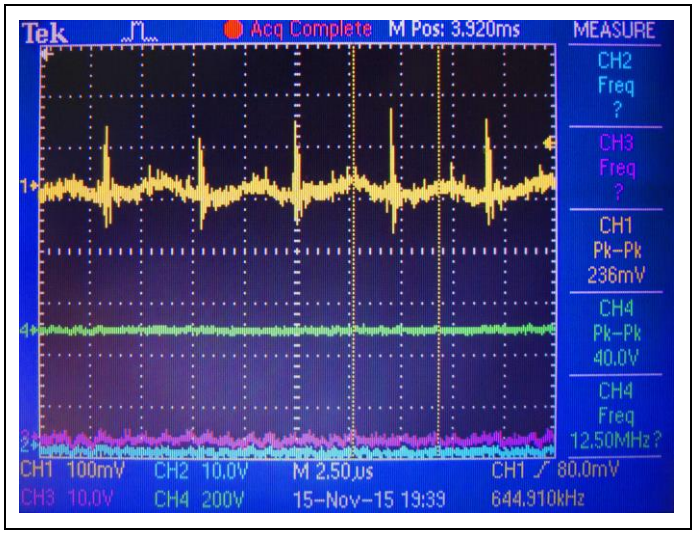

Figure 7.12: Output Voltage Ripple.

- Channel 1 : Output Voltage

7.3.4. ZVS for Switching MOSFETs

Because of the phase shift between the current and voltage of the resonant tank the MOSFETs switch without any losses during turn on transition as shown in Figure 7.13.

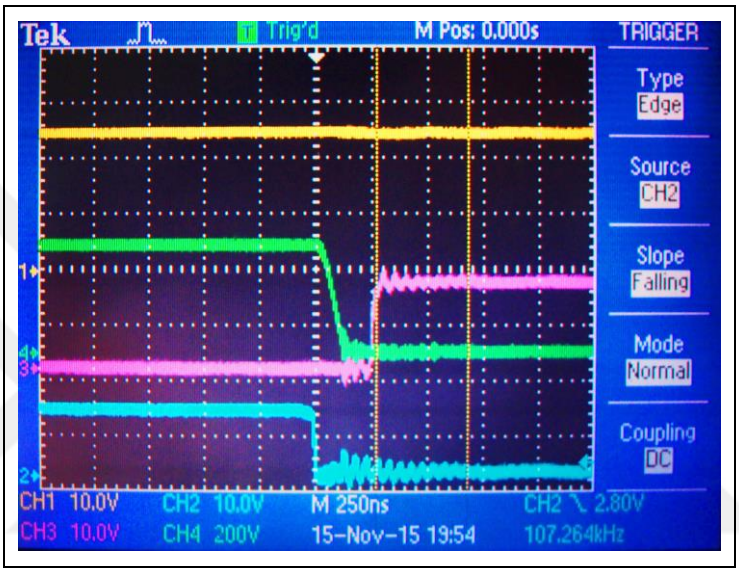

Figure 7.13: ZVS for High Side MOSFET Q1.

- Channel 1 : Output Voltage
- Channel 2 : Gate to Source Voltage of the MOSFET Q2
- Channel 3 : Gate to Source Voltage of the MOSFET Q1
- Channel 4 : V_{ds} (Drain to Source Voltage for the MOSFET Q1)

7.3.5. ZCS for Secondary Rectifier

Figure 7.14 demonstrates zero current switching operation on the secondary rectifier during turn off transition.

Figure 7.14 ZCS for Secondary Rectifier.

- Channel 2 : Secondary Diode Voltage
- Channel 4 : Secondary Diode Current

7.3.6. Primary MOSFET Current

High side MOSFET Q1 current is demonstrated at light load and full load conditions in Figure 7.15 and Figure 7.16, respectively.

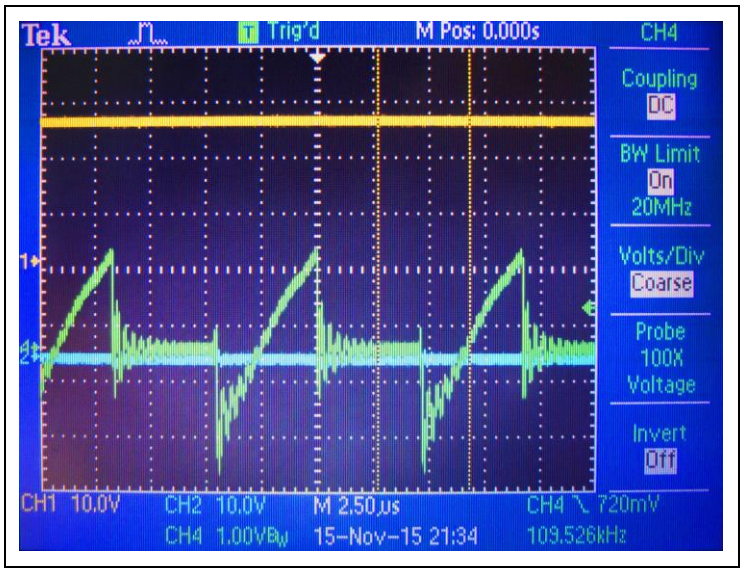

Figure 7.15: Primary MOSFET Q1 Current at Light Load.

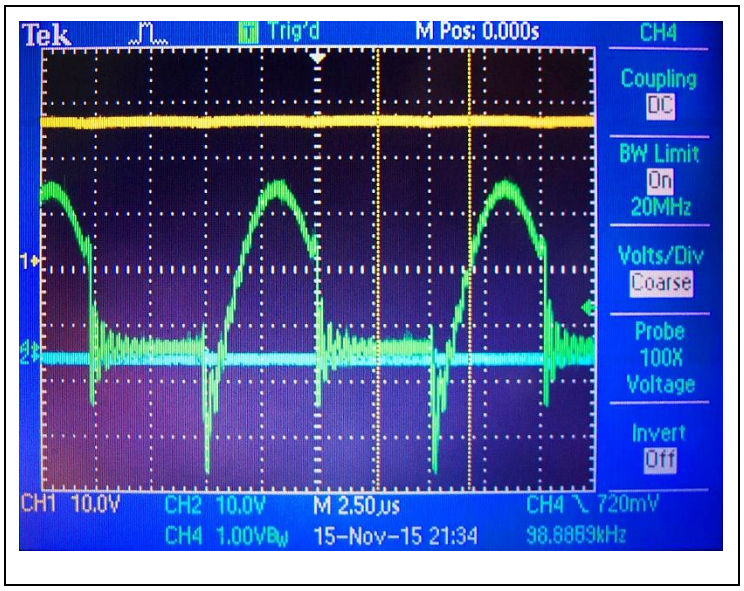

Figure 7.16: Primary MOSFET Q1 Current at Full Load.

- Channel 4 : Q1 MOSFET Current

7.3.7. Resonant Tank Current

Figure 7.17 and Figure 7.18 shows the resonant tank current under light load and full load conditions, respectively.

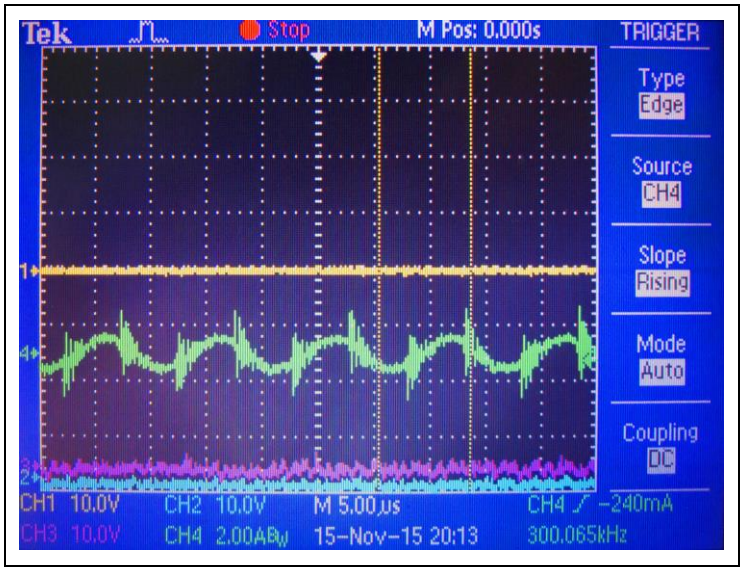

Figure 7.17: Resonant Tank Current at Light Load.

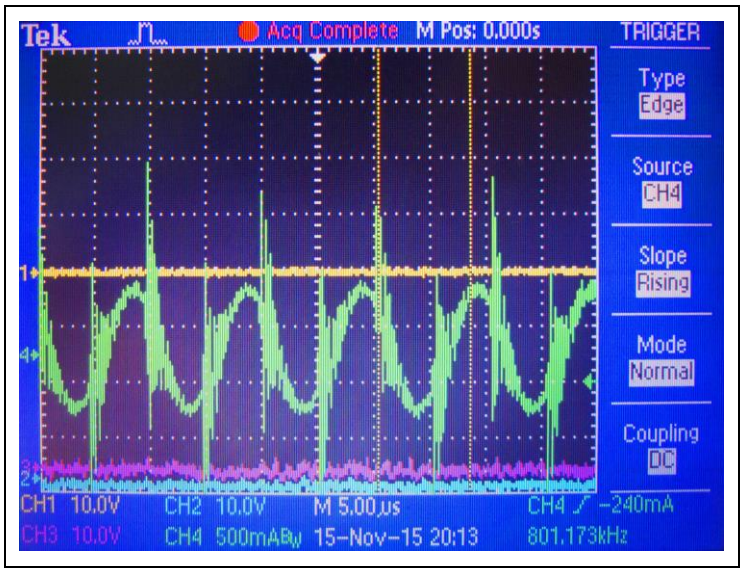

Figure 7.18: Resonant Tank Current at Full Load.

- Channel 4 : Resonant Tank Current

7.3.8. Secondary Side I-V Relationship

Figure 7.19 and Figure 7.20 shows the secondary side I-V relationship under light load and full load conditions, respectively.

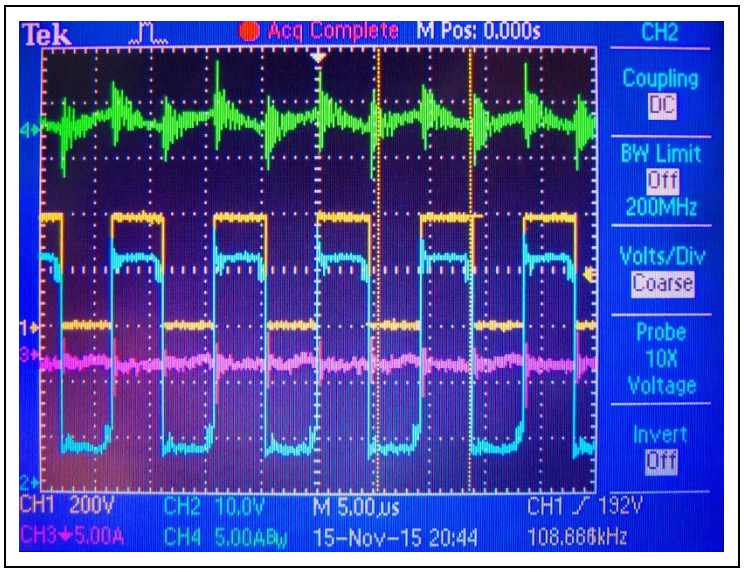

Figure 7.19: Secondary Side I-V Relationship at Light Load.

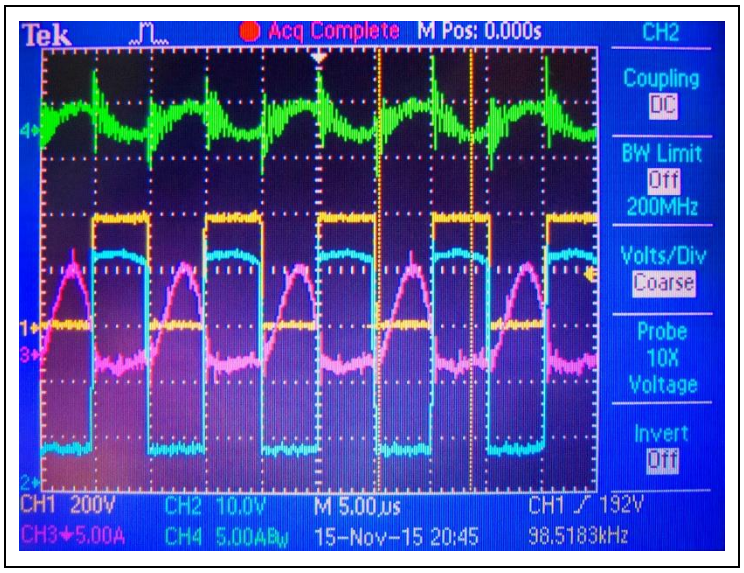

Figure 7.20: Secondary Side I-V Relationship at Full Load.

- Channel 1 : Gate to Source Voltage of the MOSFET Q1
- Channel 2 : Secondary Diode Voltage
- Channel 3 : Secondary Diode Current

8. CONCLUSION

An LLC half-bridge resonant converter is designed and implemented with digital control for the uni-directional DC-DC converter. The converter principles are presented using First Harmonic Approximation model and transfer function equations is obtained using the model. The fundamental operation modes are analyzed with the voltage-current waveforms. The reactive components are calculated by the aid of the design procedure.

The converter design is then simulated in LTSpice IV with the designed components. Using the hardware simulations, digital controller is designed and tuned in order to provide soft start, minimum settling time, overshoot, undershoot, steady state error and better load response. The controller is simulated with Matlab® Simulink® and simulation results are presented.

In order to verify hardware and digital controller simulations, the complete designed resonant converter is implemented practically and experiments are performed to demonstrate the proposed converter design is giving the expected results. Experimental test results show that the output voltage and current are adjusted by varying the switching frequency away from the resonance point and ZVS and ZCS are provided in the primary and secondary side of the transformer.

REFERENCES

Buccella C., Cecati C., Latafat H., Razi K., (2012), "Digital Control of a Half-Bridge LLC Resonant Converter", 15th International Power Electronics and Motion Control Conference, LS6a.4-1 - LS6a.4-6, Novi Sad, Serbia, 4-6 September.

Brocard G., (2011), "The LTspice IV Simulator", 1st Edition, Würth Elektronik eiSos GmbH co. KG.

Chen H., (2012), "LLC Resonant Current Doubler Converter", Master's Thesis, University of Canterbury.

Chen Y., Liang T., Tseng W., Lee J., Yang L., (2010), "Design and Implementation of LLC Resonant Converter with High Efficiency at Light Load Condition", 2nd IEEE International Symposium on Power Electronics for Distributed Generation Systems Design, 538-542, Hefei, China, 16-18 June.

Corradini L., Maksimovic D., Mattavelli P., Zane R., (2015), "Digital Control of High-Frequency Switched-Mode Power Converters", 1st Edition, John Wiley & Sons.

Fang X., Hu H., Shen J., Batarseh I., (2012), "An Optimal Design of the LLC Resonant Converter Based on Peak Gain Estimation", Applied Power Electronics Conference and Exposition (APEC), 1286-1291, Orlando, FL, USA, 5-9 February.

Fang Z., Duan S., Chen C., Chen X., (2013), "Optimal Design Method for LLC Resonant Converter with Wide Range Output Voltage", Applied Power Electronics Conference and Exposition (APEC), 2106-2111, Long Beach, CA, USA, 17-21 March.

Gopiyani A., Patel V., (2011), "A Closed-Loop Control of High Power LLC Resonant Converter for DC-DC Applications", Engineering (NUiCONE), Nirma University Intl. Conf., 1-6, Ahmedabad, Gujarat, India, 08-10 December.

Huang J., Wang S., Liu Y., (2011), "Design of a Digitally-Controlled LLC Resonant Converter", 2011 International Conference on Information and Electronics Engineering IPCSIT, 55-59, Singapore, 14-16 October.

Jung J., Kwon J., (2007), "Theoretical Analysis and Optimal Design of LLC Resonant Converter", 2007 European Conference on Power Electronics and Applications, 1-10, Aalborg, Denmark, 2-5 September.

Kandrac J., Frivaldsky M., Prazenica M., Simonova A., (2012), "Design and Verification of proposed Operation Modes of LLC Converter", Elektronika ir Elektrotechnika, 18 (8), 27-30.

Liu Y., (2007), "High Efficiency Optimization of LLC Resonant Converter for Wide Load Range", Master's Thesis, Virginia Polytechnic Institute.

Lu B., Liu W., Liang Y., Lee F. C., Wyk J. D., (2006), "Optimal Design Methodology for LLC Resonant Converter", Twenty First Annual IEEE Applied Power Electronics Conference and Exposition, 533-538, Dallas, TX, USA, 19-23 March.

MCI., (2010), DC/DC LLC Reference Design Using the dsPIC DSC, AN1336, Microchip Technology Inc.

ST, (2016), STM32F429xx Datasheet, STMicroelectronics.

TI, (2010), Designing an LLC Resonant Half-Bridge Power Converter, TI Power Supply Design Seminar SEM1900, Texas Instruments.

Vorpérian V., (1984), "Analysis of Resonant Converters", Doctoral Thesis, California Institute of Technology.

Web 1, (2015), http://www.powertransmission.com/issues/0411/pid.pdf, (Erişim Tarihi: 17/09/2015).

Web 2, (2015), https://www.silabs.com/marcom%20documents/resources/introto digitalcontrol.pdf, (Erişim Tarihi: 08/06/2015).

Yu R., Ho G. H., Pong B. M. H., (2012), "Computer-Aided Design and Optimization of High-Efficiency LLC Series Resonant Converter", IEEE Transactions on Power Electronics, 27 (7), 3243-3256.

BIOGRAPHY

Serkan DOĞANGÜNEŞ was born in Ankara in 1988. He received his B. Sc degree in Electronics And Communications Engineering from Yıldız Technical University in 2011. In 2013, he started M.Sc. degree at Gebze Technical University in Graduate School Of Natural And Applied Sciences, Department Of Electronics Engineering. He works currently as electronics design engineer in avionics and military projects.